J Mater Sci (2010) 45:6283–6312
DOI 10.1007/s10853-010-4509-1

IMEC 2009

Science and engineering of electrospun nanofibers for advances in clean energy, water filtration, and regenerative medicine

S. Ramakrishna · R. Jose · P. S. Archana · A. S. Nair · R. Balamurugan · J. Venugopal · W. E. Teo

Received: 15 January 2010 / Accepted: 9 April 2010 / Published online: 27 April 2010

Abstract Nanostructured materials with high aspect ratio and one-dimensional (ID) morphology are nature's choices when high degree of functional performances and flexible properties are concerned. Two examples are extracellular matrices in tissues of living organism, and light harvesting rods of the retina and chlorophyll. Electrospinning (E-spinning) is a simple processing technique that allows fabrication of high aspect ratio nanofibers (NFs) in a commercial scale. Electrospun nanofibers (E-spun NFs) combine a number of physical properties such as guided electron transport, strain-induced electronic properties, high mechanical strength, high degree of flexibility, large specific surface area, high electron and thermal diffusivity, and tailorable pore distribution. Our laboratory has been involved in fabrication of E-spun polymeric, inorganic, and polymer-nanocomposite fibers in random, aligned, cross-aligned, sheaths, tubes, yarns, core/shell, and trilayer morphologies. This article focuses on application of the E-spun fibers in the areas of clean energy, water treatment, and regenerative medicine in the authors' laboratory. In addition, the article briefly reviews the progress made in these areas using E-spun NFs.

S. Ramakrishna (✉) · R. Jose · P. S. Archana · A. S. Nair · R. Balamurugan · J. Venugopal · W. E. Teo
Healthcare and Energy Materials Laboratory, National University of Singapore, 117576 Singapore, Singapore
e-mail: seeram@nus.edu.sg

S. Ramakrishna
Institute of Materials Research and Engineering (IMRE), A-STAR, 3 Research Link, 117602 Singapore, Singapore

S. Ramakrishna
King Saud University, Riyadh 11451, Kingdom of Saudi Arabia

R. Jose
Faculty of Industrial Science and Technology, Universiti Malaysia Pahang, 26300 Pahang, Malaysia

Introduction

One-dimensional (ID) nanostructures are choice of the nature when high degree of functional performances and flexible properties are concerned as in extracellular matrices, neural networks, and light harvesting rods of the retina and chlorophyll. Fabrication of 1D structures of the new generation materials could, therefore, provide new opportunities to improve and/or modify performances of the advanced functional devices and structures. Electrospinning (E-spinning), which works under the principle of asymmetric bending of a charged liquid jet when accelerated by a longitudinal electric field, is a technique that allows fabrication of continuous NFs of polymers and advanced functional materials. In the E-spinning process, a polymer solution is injected from a needle in the presence of an electric field. When the applied electric field overcomes surface tension of the liquid, a continuous jet is ejected, which on subsequent solvent evaporation and bending produces NFs on a collector surface [1]. Figure 1 shows a schematic of the processes during E-spinning. Various fiber morphologies could be produced by E-spinning such as random, aligned, core–shell, bundles, and mats, and these are done by merely changing the collection and/or injection strategy [2–5]. If the polymer solution contains respective metal ions for forming an inorganic solid, then appropriate post-electrospinning heat treatment yields continuous inorganic NFs [6, 7].

The E-spinning as a method to produce continuous fibers has been known since 1902 [8]. Figure 2 shows the E-spinning timeline showing its evolution as an acceptable

technology since its inception. There is a revived interest in E-spinning in academia from mid-1990s with the advances in nanotechnology [9], which is possibly due to the potential of the process to fabricate 1D nanostructures of a wide range of materials systems.

E-spun NFs (NFs) have interesting physical characteristics: (i) high specific surface area and interesting pore distribution; (ii) polymer NFs are opaque due to high packing density of monomers; and (iii) metal oxide NFs are with controllable crystallinity and are characterized by diameter-dependent strain. The E-spun NFs of lead zirconate titanate showed a piezoelectric response that is ~200 times higher than that of corresponding single crystals [10]. High efficiency photovoltaic devices were also demonstrated using E-spun metal oxide NFs [11] in addition to study some of the factors affecting the conversion efficiency of dye-sensitized solar cells (DSCs) [12]. Owing to their high scientific and commercial potentials, E-spinning as a method for producing 1D nanostructures is gaining increased interest both in academia and industry. Applications envisaged using E-spun NFs since its discovery are summarized in Fig. 3.

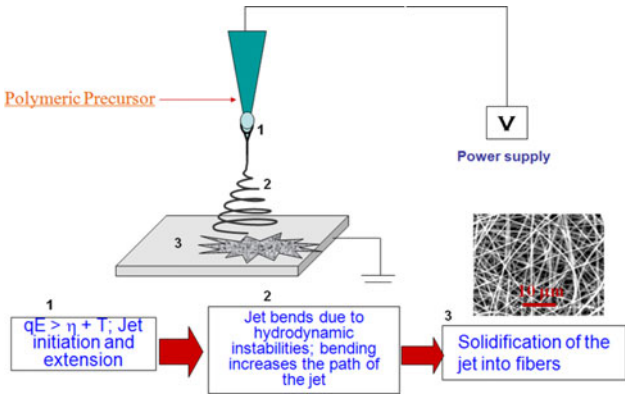

Fig. 1 Schematics of the electrospinning (E-spinning) process. The experimental set-up consists of a high voltage power supply, a spinneret, and a collector. The three processes, viz., formation of tailor cone (1), bending due to various instabilities (2), and collection of solid samples (3) are shown. The qE is the electrostatic force, η is the viscosity, and T is the surface tension. Conventionally, E-spinning produces a fiber cloth consisting of randomly oriented nano/microfibers, a typical SEM image of which is also shown

Studies have been carried out in our laboratory to utilize E-spun NFs to address global challenges requiring immediate attention such as clean energy, water treatment, and regenerative medicine. This article is organized to provide an overview of advances in E-spinning and the application of NFs in the areas of photovoltaics, water filtration, and healthcare. "Electrospun nanostructures for energy conversion and storage" section of this article deals with application of E-spun TiO_2 nanostructures in energy, both photovoltaic and lithium ion batteries (LIBs), starting from global energy scenario; "Nanofibers for water filtration" section focuses on the application of E-spun membranes for water filtration; and "Nanofibers for regenerative medicine" section concentrates on their applications in regenerative medicine. Notable drawbacks of E-spinning are also included. A brief summary, future prospects, and limitations are given at the end of each section.

Fig. 2 Electrospinning timeline

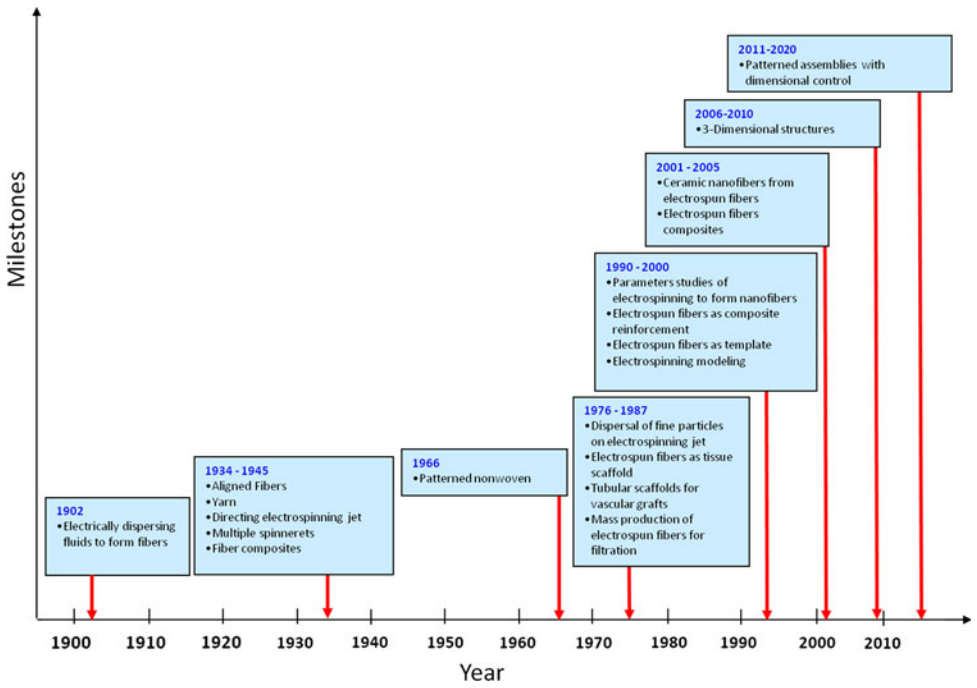

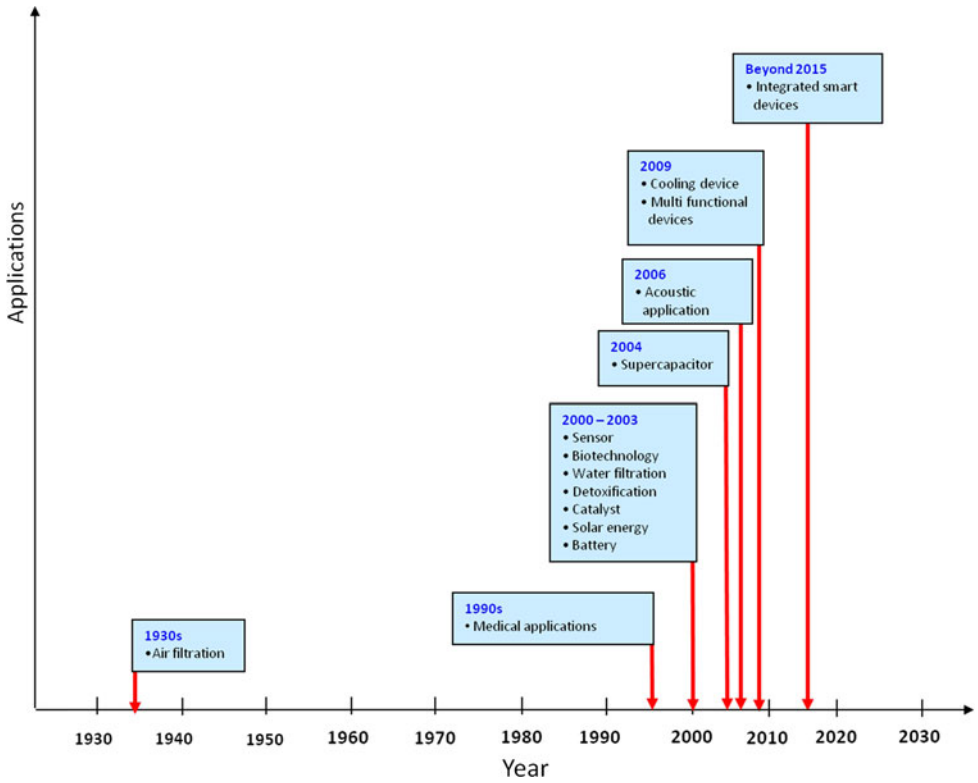

Fig. 3 Application domains where E-spun NFs could be used. Next generation devices employing E-spun NFs are predicted in the area of integrated smart devices making use of organic–inorganic interfaces and functional films

Electrospun nanostructures for energy conversion and storage

Energy scenario

Nanostructured materials are characterized by large specific surface area which enables to reduce the quantity of materials required to fabricate a device. Moreover, they possess enhanced and/or modified physical properties that increase and/or modify the functionalities of the devices. These two factors, viz., lower material requirements and improved/modified functionality, combine to fuel the motivation of research on nanostructured materials for energy conversion.

Owing to an increasing population together with improved living standards expected for most people, energy consumption will increase drastically with time. Figure 4 is an excerpt from a book titled "Changing Face of Innovation: Is it Shifting to Asia" showing the energy supply and shares [13]. The modern society heavily relies on fossil fuels for electricity generation and transportation. Energy obtained from the combustion of fossil fuels leave us vulnerable to green house gasses, which cause severe health hazards, and global warming. The realization of these long-term ill effects made scientists to look for several clean energy conversion techniques some of which include nuclear energy, hydroelectricity, tidal energy, solar energy, and electrochemical energies. More solar energy strikes the Earth in one hour (4.3×10^{20} J) than all the annual human energy consumption (4.1×10^{20} J) [14]. Harvesting this clean energy and converting into electrical power is the science and technology behind photovoltaics, which is an intensely and hotly pursued research topic in recent times.

Renewable energies are clean but are less convenient to use; the main constraint is that the energy sources such as solar light or wind are not always available. Energy consumption does not match with the availability of sun or wind; for example, energy demand is high after sunset to provide lighting. Therefore, renewable energy is featured with dual topic: energy generation and storage, i.e., energy is produced when possible and stored until it is needed. Rechargeable lithium batteries [15] and electrochemical double layer capacitors (supercapacitors) [16] are two protocols gaining recent attention to store energy with high power, capacity, and safety. The LIBs provide the highest energy density (150–200 Wh/kg), but at the expense of cycle life ($<10^3$ cycles); whereas, supercapacitors exhibit the highest known power capability (2–5 kW/kg) and long cycle life (10^4–10^6 cycles), but suffer from a modest energy density (3–6 Wh/kg). The energy storage devices fabricated using nanostructured materials have higher capacities and rate capabilities due to their higher surface area than that of the bulk counterparts. In addition, the nanostructured materials reduce the overpotential and allow faster reaction kinetics at the electrode surface.

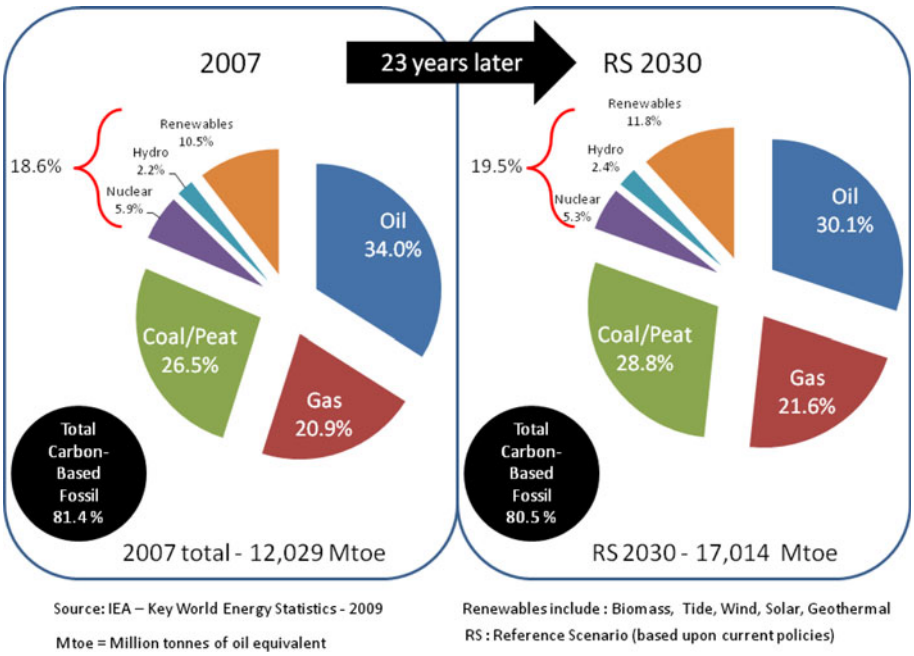

Fig. 4 Fuel share for primary energy supply [13]. The figures were from those authors' study

In the next sections, detailed descriptions on these two types of energy devices fabricated using E-spun NFs are given.

Solar energy conversion—the dye-sensitized solar cells

Currently available solar cells can be broadly classified into *p–n* junction solar cells and excitonic solar cells (ESCs) [17]. In the *p–n* junction cells, the photogenerated electrons are accelerated by a built-in electric field at the junction between the *p*- and the *n*-type semiconductors. In the ESCs, light absorption results in the generation of excitons, which are quasi particles with an electron in the conduction band (or the lowest unoccupied molecular orbital, LUMO, in the case of molecules and clusters) and a hole in the valence band (or the highest occupied molecular orbital, HOMO, in the case of molecules and nanoclusters). The excitons thus generated in a semiconductor are dissociated at a material interface into free carriers in excitonic solar cells. Popular examples of excitonic solar cells are the DSCs [18], organic solar cells [19], and quantum dot solar cells [20]. Organic solar cells employ conjugated conducting polymers and/or organic materials. The photovoltaic effect in DSC occurs at the interface between a dye-anchored wide bandgap oxide semiconductor and an electrolyte. In quantum dot solar cells, semiconductor nanocrystals with sizes less than their exciton's Bohr radius have been used to harvest light, i.e., the quantum dots simply replace dyes, so far.

The DSCs are fabricated by (i) sintering a wide bandgap metal oxide semiconductor, typically mesoporous TiO_2, on a conducting glass plate, usually fluorine-doped tin oxide (FTO); (ii) dye anchoring on the sintered metal oxide layer; (iii) counter electrode fabrication, which is typically a Pt sputtered FTO; (iii) sealing; and (iv) electrolyte filling. The optimized processes for fabrication of highly efficient

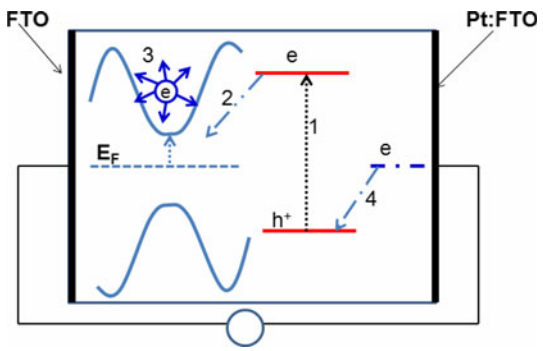

Fig. 5 Typical materials' arrangement and processes in DSCs. Light absorption by the dye results in an electron at the unoccupied molecular orbital of the dye leaving a hole at its occupied molecular orbitals (process 1). The photogenerated electrons are then injected to the metal oxide semiconductor (process 2) due to the overlapping of the wave functions [12] achieved through chemisorption of the dyes on the metal oxide. The photoelectrons received by the metal oxide cause its Fermi level to rise and subsequently result in photoconductivity. In metal oxides, the electron diffuses randomly; the surviving electrons are collected, and they use their energy to do an external work and then deliver them at the counter electrode, from where they are injected to the dye to neutralize the hole. Catalysts are used at the counter electrode, usually platinum, for faster regeneration of the dye. The random electron diffusion imposes severe restrictions on the scalability of the DSCs as the chances of collecting the electrons decreases with increase in the device area. One dimensional metal oxides are likely a remedy to increase the charge collection and scalability of the device

Table 1 Solar energy conversion efficiencies of various solar cells at cell (area <1 cm2), submodule (area <25 cm^2), and modules (area >50 cm^2). The table is summarized from the recent photovoltaic update provided by Green et al. [24]

Type of cell	Description	Efficiency (%) at AM1.5 spectrum	
		Without concentrator [area (cm^2)]	With concentrator [area (cm^2), intensity (suns)]
p–n (Single junction)	Silicon		
	Crystalline	25.0 ± 0.5 [4.00 (da)]	27.6 ± 1 [1.00 (da), 92]
	Polycrystalline	20.4 ± 0.5 [1.002 (ap)]	
	Amorphous	9.5 ± 0.3 [1.070 (ap)]	
	Nanocrystalline	10.1 ± 0.2 [1.199 (ap)]	
	GaAs		
	Thin film	26.1 ± 0.8 [1.001 (ap)]	28.8 ± 1.2 [0.0504 (da), 232]
	Polycrystalline	18.4 ± 0.5 [4.011 (t)]	
	InP		
	Crystalline	22.1 ± 0.7 [4.02 (t)]	
p–n (Multi junction)	GaInP/GaAs/Ge	32.0 ± 1.5 [3.989 (t)]	40.7 ± 2.4 [0.267 (da), 240]
			20.7 ± 1.5 [34 (da), 10]
	GaInP/GaAs	30.3 [4.0 (t)]	
	GaInP/GaInAs/Ge		41.1 ± 2.5 [0.0509 (da), 454]
Thin film	$CuInGaSe_2$ (cell)	19.4 ± 0.6 [0.994 (ap)]	21.8 ± 1.5 [0.102 (da), 14]
	$CuInGaSe_2$ (submodule)	16.7 ± 0.4 [16.0 (ap)]	
	CdTe	16.7 ± 0.5 [1.032 (ap)]	
	Si	16.7 ± 0.4 [4.017 (ap)]	
	Si (submodule)	10.5 ± 0.3 [94.0 (ap)]	
Excitonic	Dye solar cells (cell)	11.2 ± 0.3 [0.219 (ap)]	
	Dye solar cells (submodule)	8.4 ± 0.2 [17.11 (ap)]	
	Organic polymer	5.15 ± 0.3 [1.021 (ap)]	
	Organic (submodule)	2.05 ± 0.3 [223.5 (ap)]	

Da designated illumination area, *ap* aperture area, *t* total area

DSCs were recently published [21]. The reader may refer to the processes and rate limiters in DSCs in recent reviews [22, 23]. In brief, upon irradiation, the electrons in the dye are excited to the higher energy levels from where they are injected into the metal oxide (Fig. 5) due to the overlapping of their electronic wave functions. These electrons are transported through the metal oxide and collected by the FTO, which is coated with a thin layer (≤100 nm) of TiO_2 that acts as blocking layer to the holes. Role of the electrolyte is two-fold: (i) regeneration of the dye, and (ii) blocking electrons from reaching the counter electrode. It should be noted that the photoconversion efficiency (η) of DSCs is much higher than that of the other ESCs and *p–n* junction solar cells fabricated using amorphous or nanocrystalline silicon [24]. Certified η as high as 8.4% in submodules [25] (area ~18 cm^2) and 11.5% in laboratory scale (area ~0.22 cm^2) has been achieved using mesoporous TiO_2-based DSCs [24, 26]. The DSCs have the potential for becoming cost-effective means for producing electricity, capable of competing with available solar electric technologies and, eventually, with today's conventional power technologies [27]. An update of photovoltaic conversion efficiencies of various solar cells at single cell, submodule, and module levels with or without solar concentrators is summarized in Table 1.

Role of 1D nanostructures in DSCS

It is generally accepted that photoelectrons injected into mesoporous TiO_2 in the DSCs move via trap-limited diffusion process [28–34]; i.e., the electrons undergo a series of trapping and detrapping events as the energy states lie within the bandgap during diffusion. These inner-lying energy states are a characteristic of the nanomaterials which are arising from an increased number of defects such as packing defects, unsaturated bonds, and deviation from the bulk long-range order [22, 28, 35]. The trapping and detrapping events result in lower electron mobility (μ_n) and diffusivity (diffusion coefficient, D_n) than the bulk materials and thereby increasing the diffusion time [28]. Longer diffusion time causes the electrons to undergo a series of recombination processes with electrolyte, oxidized dye,

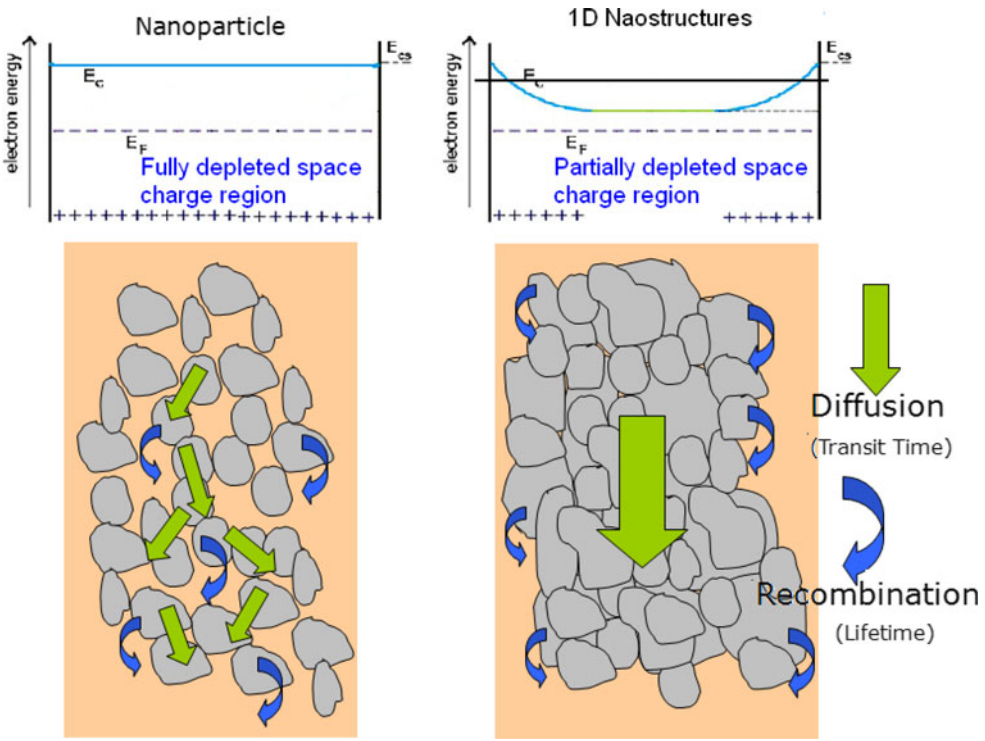

Fig. 6 Differences in the diffusion process between nanoparticles and 1D morphologies. The nanoparticles are too small to support macroscopic electric fields; therefore, the charge transport is diffusion limited. On the other hand, 1D nanostructures with solid cross section can have a partially depleted space charge region. Band edge type conduction, similar to bulk semiconductors, could be expected from the 1D nanostructure. Besides, sintering of mesoporous particles leaves pores that increases the recombination pathways which is reduced in 1D nanostructures

and phonon relaxation [22]. The distance traveled by the electrons before being recombined is known as the diffusion length, $L = \sqrt{D_n \tau}$, where τ is the electron lifetime, which for conventional nanoparticle-based DSCs is $L \sim 30$ μm [36]. The film thickness should be $\sim L/3$ for efficient charge collection.

Hence, an increase in the nanoparticle film thickness significantly above 10 μm does not increase the η. On the other hand, η of the DSCs could be increased by increasing the thickness of the mesoporous network using materials and architectures of higher D_n. As shown in Fig. 6, 1D structures, such as nanowires, nanotubes, nanorods, and NFs in the place of nanoparticles, have been proposed to have longer L due to the directed charge transport through them [37–42]. There are two types of these 1D nanostructures: (i) ordered nanotube or nanowire arrays vertically aligned on conducting glass substrates and (ii) random network of 1D nanostructures. While ordered structures are attractive in terms of the device performance parameters, such as diffusion length and time, their scalability is a major issue. On the other hand, disordered structures could be developed in large scale through nanofabrication techniques such as E-spinning. TiO_2 is an archetypical nanostructure exploited for the DSC application; therefore, this article is restricted on the synthesis of 1D TiO_2 nanostructures by E-spinning, characterization of the resulting nanostructures and evaluation of their properties, as well as device fabrication and testing.

TiO_2 nanofibers by E-spinning

The TiO_2 NFs were first prepared using E-spinning by Li and Xia in 2003 [43]. Those authors have dispersed a sol of titanium isopropoxide [Ti(*i*PrO)$_4$] in poly(vinyl pyrrolidone) (PVP), and the resultant solution was E-spun to prepare polymeric NFs which upon heat treatment produced continuous NFs of TiO_2. The diameter of the final TiO_2 NFs was controlled through varying the solution viscosity, solution feed rate, intensity of the electric field, and concentration of the Ti(*i*PrO)$_4$ precursor [43]. Decomposition of the composite fiber in which Ti ions are dispersed in PVP and crystallization behavior are determined by simultaneous differential thermal (DTA) and thermogravimetric analysis (TGA) (Fig. 7). The thermal analyses showed an exothermic event in the DTA curve and a weight loss (~20%) in the TGA curve at ~60 °C. These events result from the liberation of surface-adsorbed ethanol. Although the bending instabilities during the E-spinning increases the jet path length enormously which helps in solvent evaporation and subsequent solidification, a small amount of solvent is expected to adhere to the surface. Following the exothermic event at 60 °C, a major endothermic event and substantial weight loss (35%) were observed at ~300 °C, which results from crystallization of the anatase phase and/or decomposition of the polymer. Wang et al. [44] showed that crystallization of TiO_2 in E-spun PVP occurs at ~210 °C using 1-tetra-*n*-butyl

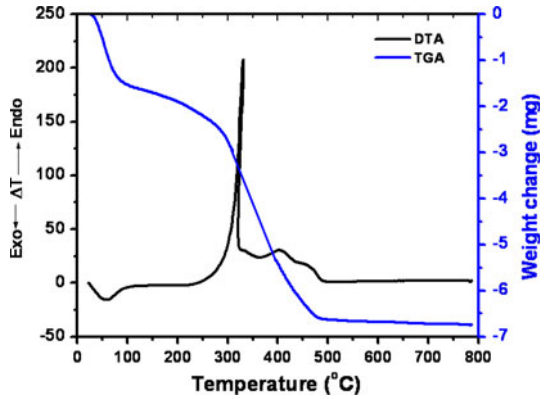

Fig. 7 Simultaneous thermal analysis of the composite fiber where a sol for TiO_2 is uniformly dispersed in PVP

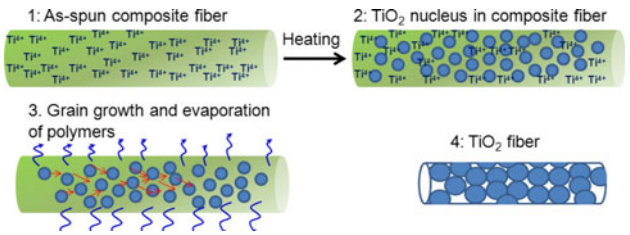

Fig. 8 Cartoon depicting the nucleation and growth of pure TiO_2 fiber from (1) a composite fiber in which titanium ions are dispersed; (2) heating at a critical temperature leads to a threshold supersaturation for nucleation of TiO_2—nucleation of the crystals relieves the supersaturation of monomers; (3) the crystal grows from the available monomers, and the grains undergo a directional mass transport with simultaneous evaporation of polymers; and (4) the crystals ultimately form pure TiO_2 NFs. Although the E-spinning is a top-down approach for nanofabrication, the formation of an inorganic species from the polymeric fiber follows bottom-up principles

titanate as the titanium precursor; therefore, the present assignment is acceptable. Two more endothermic events are observed in the DTA curve, which are believed to arise due to the complete decomposition of the leftover polymer and grain growth, respectively.

From the observed thermal analyses' curves, formation of metal oxides from the composite polymer on heat treatment involve at least three processes, viz. (i) nucleation of the crystals, (ii) growth, and (iii) directional mass transport, in other words, sintering of the grains. The first two processes typically occur during growth of nanocrystals from solutions. These processes are schematically shown in Fig. 8.

Mesoporous TiO_2 NFs with high specific BET surface area ($\sim$200 m^2/g) using a triblock co-polymer, pluronic P-123, have also been produced by E-spinning [45, 46]. Nuansing et al. [47] systematically studied the growth of TiO_2 as well as phase transition from anatase to rutile. They observed that the anatase to rutile transition occurs at temperatures <600 °C. Kumar et al. [48] showed that lowering of the anatase-to-rutile phase transition is a function of fiber diameter and arises from the increased strain due to the capillary forces. All the above studies used conventional random E-spun fiber morphology. Fabrication of well-aligned TiO_2 NFs was reported using near field E-spinning [49]. Recent articles of E-spun TiO_2 NFs or their composites with other materials have focused on the application potential of this morphology. These areas include sensing [50–53], lithium-ion batteries [54, 55], catalysis [56–59], and DSCs [12, 41, 60–66].

Morphology of the annealed TiO_2 fibers examined by field emission scanning electron microscope (SEM) and high resolution transmission electron microscope (HRTEM) is shown in Fig. 9. The NFs maintained cross-sectional uniformity throughout the length indicating a smooth injection of fine TiO_2 sol dispersed in the polymer matrix.

One of the most attracting properties of the E-spun NFs is its viability to tailor the crystallinity by controlling the solution chemistry for E-spinning [63] or heat treatment without disturbing the fiber diameter [67]. As majority of the application areas of the E-spun TiO_2 NFs, such as sensors, solar cells, and batteries, depend on the electrical resistance, the crystallinity (i.e., particle size) of the fibers is of crucial importance. Reduced crystallinity increases the grain boundaries from where electrons scatter additionally and thereby increases the electrical resistance. Figure 10 shows the HRTEM images and selected area diffraction patterns of three typical TiO_2 NFs of radius $\sim$150 nm, which display the difference in crystallinity due to heat treatment.

Crystal structure evolutions in E-spun TiO_2 nanofibers

The powder X-ray diffraction (XRD) and selected area electron diffraction (SAED) techniques are powerful tools to identify the crystal structure of the materials. Figure 11 shows the phase evolution of E-spun TiO_2 NFs as a function of heat treatment. No XRD peaks were detected for the as-spun polymeric fibers [48]. Well-crystallized pure anatase TiO_2 NFs without any polymeric part were obtained by heating the as-spun fibers at $\sim$500 °C for $\sim$60 min. The lattice parameters of the anatase phase were $a = 3.784$ Å and $c = 9.514$ Å, which are close to the earlier reported values [68].

The rutile phase was observed to nucleate and grow in the fiber at temperatures at $\sim$550 °C. The lattice parameters calculated from the rutile phase were $a = 4.594$ Å and $c = 2.959$ Å, which are also close to the earlier reported values [69]. Lowering of anatase-to-rutile phase transition temperature (T_a) was observed compared to the one observed for nanoparticles [70–73], which is assigned to

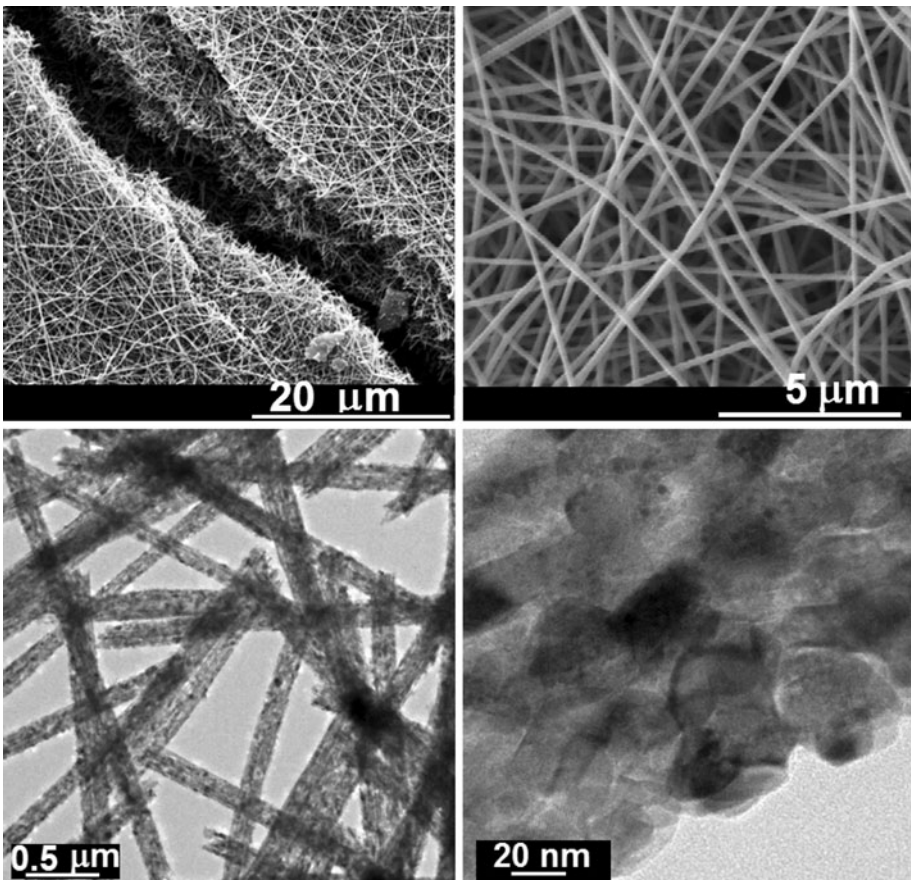

Fig. 9 *Top panel*: SEM micrograph of the TiO_2 NFs showing layers of fiber sheet and magnified portion displaying the continuous morphology. *Bottom panel*: TEM images showing the grain arrangements and interparticle porosity

the increased capillary forces acting on the fiber surface [48]. The fibers heated up to 650 °C had the presence of anatase phase although the volume fraction is less than 5%.

Fabrication of DSCs using E-spun TiO_2 nanofibers

Initial attempts to fabricate DSCs using E-spun TiO_2 NFs were directed to develop the composite polymeric NFs films on FTO and subsequent sintering. One of the crucial problems in this protocol was the development of films with appreciable thickness ($\geq$10 μm). This is because the E-spun metal oxide NFs suffer a volume decrease due to the evaporation of polymers. The final TiO_2 film shrinks as a result of this volume change and peels off from the substrate.

Continuous TiO_2 nanofibers on FTO Song et al. [74] fabricated fibrous films of polyvinylacetate (PVAc) containing Ti^{4+} by E-spinning on FTO, and the resulting films were partially dissolved using tetrahydrofuran (THF) before sintering. The sintered films showed conventional E-spun web-like fibrous structure; however, fibers had core-sheath structure similar to multi-strand electrical wires. The core-sheath fiber formation was explained as due to phase separation during gelation in the presence of moisture. The TiO_2 sol precursor is converted to TiO_2 gel when the E-spun fibers were exposed to moisture. The solidification occurred faster in the sheath, than in the core, in which the microphase separation between TiO_2 sol and PVAc solution occurred during solidification. Considerable film thickness ($\sim$20 μm) was achieved using this technique. The DSCs fabricated using the above electrode, N3 dye, and LiI/I_2 electrolyte gave the following photovoltaic properties: open circuit voltage (V_{OC}) of $\sim$0.77 V; current density (J_{SC}) of $\sim$8.67 mA/cm^2; fill factor (FF) of $\sim$60%; and η $\sim$4.01%. This team of authors has further improved the performance of DSCs by giving an additional hot pressing during the TiO_2 film fabrication stage. A record η $\sim$6.2%—with V_{OC} $\sim$0.70 V; J_{SC} $\sim$14.77 mA/cm^2; and FF $\sim$60%—was achieved in E-spun TiO_2-based quasi-solid-state DSCs [63]. Although the original web structure of the as-spun fibers was retained in the hot-pressed fiber film, each fiber was composed of TiO_2 nanofibrils of several tens of nanometer length. Very recently, this group of authors reported η of $\sim$11% similar to the conventional nanoparticulate-based DSCs optimizing the nanorod formation, purified dyes, and electrolyte composition [11].

Onozuka et al. [62] further optimized the amount of THF and dimethylforamamide (DMF) and studied the effect of processing conditions on the photovoltaic parameters. The additional treatments of the pre-deposited

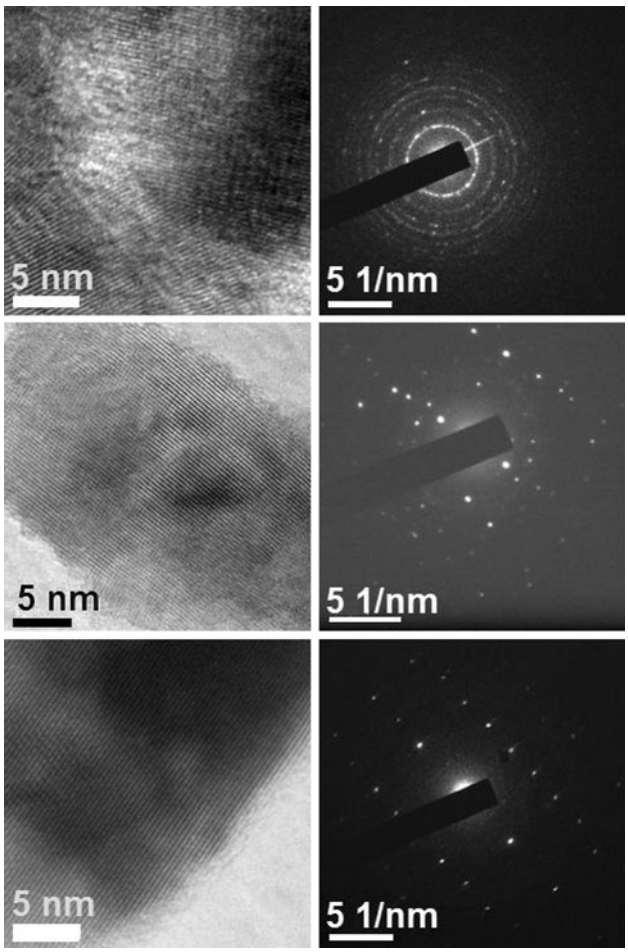

Fig. 10 HRTEM images and SAED patterns displaying increase in crystallinity of the TiO_2 NFs when the fibers are heated for prolonged duration. The figures were from those authors' study and reproduced from J Phys Chem C 113:21538, 2009 with permission

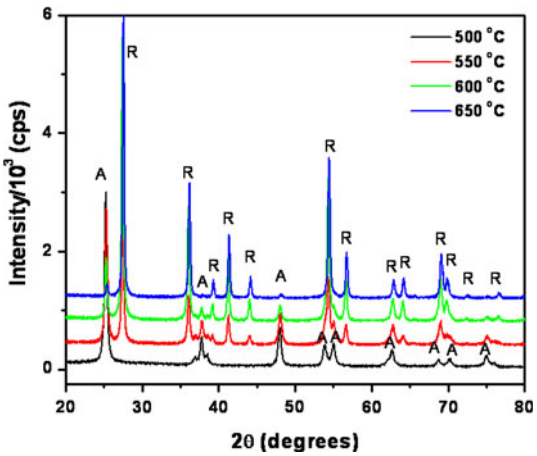

Fig. 11 XRD patterns showing the evolution of anatase and rutile phases. The A's in the figure indicate the anatase phase, and the R's indicate the rutile phase

TiO_2 film and the adhesion treatment using DMF were shown to be efficient for improving the photoelectric characteristics of the DSCs. A high J_{SC} of $\sim$9.88 mA/cm^2 and η $\sim$4.14% were obtained for relatively lower TiO_2 film thickness ($\sim$3.9 μm). Kokubo et al. [65] studied the dependence of pressure used during the hot-pressing stage on the photovoltaic parameters. The DSCs fabricated using TiO_2 films of thickness $\sim$9.2 μm obtained by pressing the composite fiber films at 8 MPa, N3 dye, and LiI/I_2 electrolyte gave V_{OC} $\sim$0.73 V, J_{SC} $\sim$16.09 mA/cm^2, FF $\sim$49%, and η $\sim$5.77%. A high J_{SC} observed in this study was a result of an enhanced BET surface area ($\sim$100 m^2/g) of the resulting films. Rui et al. [75] fabricated TiO_2 NFs films on FTO by directly E-spinning the polymeric solution on in situ-heated FTO and subsequent sintering. A thickness of $\sim$1 μm was achieved by repeating the above E-spinning–sintering steps for a number of times. Increasing the fiber thickness caused the NF films to peel off from the substrate. The solid-state DSCs fabricated using N719 dye anchored to the TiO_2 electrode and poly(3-hexylthiophene-2,5-diyl) (P3HT) as the hole-conductor gave J_{SC} of $\sim$1.3 mA/cm^2 and η of $\sim$0.3%.

Shim et al. [76] fabricated aligned and cross-aligned TiO_2 NFs on FTO by E-spinning and fabricated solid-state DSCs using poly[2-methoxy-5-(2′-ethyl-hexyloxy)–1,4-phenylene vinylene] (MEH–PPV) and poly(3,4-ethylenedioxythiophene)–poly-(styrenesulfonate) (PEDOT–PSS). The J_{SC} ($\sim$1.2 mA/cm^2) and η ($\sim$0.5%) of the aligned and cross-aligned NFs were 50% higher than that of the random NFs. It was concluded that the power conversion efficiency could be significantly improved by at least 70% under one sun condition depending on the degree of aligning TiO_2 nanowire arrays through enhancing charge collection and transport rate, as well as facilitating the polymer infiltration as compared to the random counterparts. Despite this promising result, no further efforts could be found in the published literature on the use of aligned NFs for DSC applications.

Charge transport through continuous TiO_2 nanofibers on FTO There are two types of charge movement in DSCs, viz. (i) charge transport, which refers the motion of charge through a single chemical species such as TiO_2 and (ii) charge transfer, which is charge motion through an interface. This article focuses only on charge transport through the E-spun NFs. A large number of factors affect the charge transfer in DSCs, which is the subject of a recent review [23]. Mukherjee et al. [41] recently reported charge transport behavior through random NF DSCs. The device was prepared by developing continuous TiO_2 NFs on FTO substrates duly spun coated with a thin ($\sim$100 nm) layer of TiO_2 nanoparticles and subsequent sintering. The TiO_2 NFs were polycrystalline with diameter $\sim$150 nm composing of

particles of size ~12–15 nm. The η of the resulting device was 4.2% with J_{SC} ~9.45 mA/cm^2, V_{OC} ~0.78 V, and FF ~57%. The electrochemical impedance spectroscopic (EIS) investigations of the above cell revealed that the charge transport resistance of the NF samples is lesser compared to the spherical nanoparticles. The lower transport resistance could be attributed to the one-dimensionality of the NFs. However, the D_n of the continuous NFs was slightly lesser than that of the random nanoparticles reported by Wang et al. [77]. The lowering of the D_n followed from longer transit time (~100 ms). It means that the enhanced charge collection due to the continuous NFs that are parallel to the substrate effectively reduced the D_n despite of its lower transport resistance. However, inferior crystallinity of the TiO_2 films adversely decreased the electron lifetime; and therefore, increased the recombination pathways in the NF cell. According to the transmission line model, charge transfer resistance and capacitance indicate the rate of recombination with the electrolyte. The charge transfer resistance of the NF-based cell was lower compared to the nanoparticle-based cell. The capacitance of the NF-based cell was nearly an order of magnitude higher than that of the nanoparticle cell. The E-spun NFs have a diameter large enough to support a radial electric field and thus should exhibit space charge capacitance in parallel with the capacitance from electronic states. The decreased charge transport resistance was explained as a consequence of this space charge-depleted region [67].

The electron lifetime measurement using EIS and V_{OC} decay (OCVD) measurements showed that the charge transport mechanism through NF DSCs is similar to that through nanoparticle-based ones, i.e., by trappining–detrapping mechanism. The OCVD measures the electron lifetime as a function of Fermi level or V_{OC} [34, 78]. Figure 12 shows the OCVD curve of the NF-based DSCs [41] compared to that of the nanoparticles [34] and other 1D nanostructures such as TiO_2 nanotubes [39]. While the electron lifetime showed a linear dependence on quasi-Fermi level in single crystalline nanotubes [39], it showed an exponential dependence in nanoparticles and E-spun NFs indicative of the trap-limited diffusion process. A clear increase in electron lifetime was observed in the NF-based cell whose magnitude was larger than the corresponding event in the nanoparticle-based cell. This increase in lifetime is due to high density of trap states in the nanocrystalline materials; the mobile electrons live longer times in the trap states and directly undergo recombination before they are detrapped by thermal excitations. Consequently, the conversion efficiency decreases. It is worth noting here that Song et al. reported relatively higher efficiency in single crystalline nanorods [11, 63]. Most frequently used method for improving the crystallinity is by heat treatment for longer duration; however, this would lead to an increase in the sheet resistance, as the E-spun NFs deposited on FTO, if heated for extended duration, ultimately increases the series resistance and loss of efficiency.

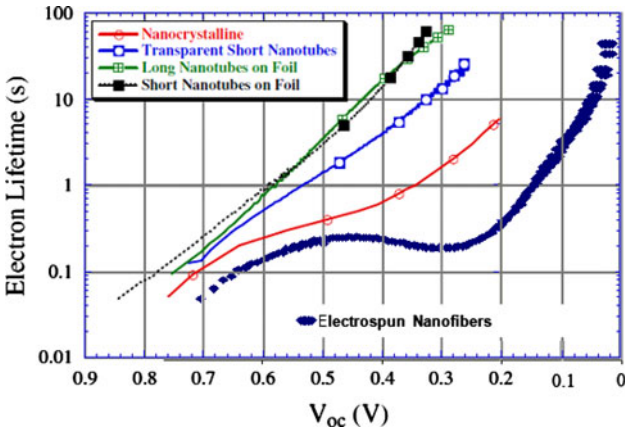

Fig. 12 The OCVD curves for various nanostructures. The OCVD curve of the NFs is from this study, whereas the others are reproduced from J Phys D Appl Phys 39:2498–2503, 2006 with permission

Ex-situ annealed fibers on FTO

In order to increase the crystallinity and thereby improve the charge transport, we have developed methods for deposition of the ex-situ-annealed NFs on FTO [61, 67]. In this method, the E-spun NFs were heated for longer duration and then either were mechanically ground to short nanorods (NRs) (aspect ratio ~1:3) [61] or ultrasonically dispersed in a solution to nanowires (NWs, aspect ratio ~1:10) [67]. These NWs and NRs were developed into a film on FTO by conventional film fabrication processes such as spray deposition or doctor blade technique [12, 60, 61, 67]. As shown in Fig. 13, no appreciable change in the fiber diameter was observed when prolonging the heating; however, their crystallinity could be greatly increased. The crystallinity of the fibers increased considerably due to grain growth from ~10–15 nm (1 h) to 25–50 nm (24 h), which was well reflected in the SAED patterns and HREM images. Microstructure of typical NWs obtained using the annealed fibers after ultrasonication are in Fig. 14.

The ex-situ annealing and subsequent film fabrication have several advantages compared to those using direct spinning of film on FTO; most important one is the viability for large area of deposition of thicker films (thickness >10 μm) with higher degree of uniformity. In addition, tailoring the charge transport properties is possible by controlling the aspect ratio of the fibers. With regard to the charge transport properties, Archana et al. [67] recently showed enhanced D_n in NW films fabricated using ex-situ-annealed TiO_2 NFs compared to those of the continuous NFs. Furthermore, the D_ns of the 24-h heated samples determined using the transient photocurrent measurements

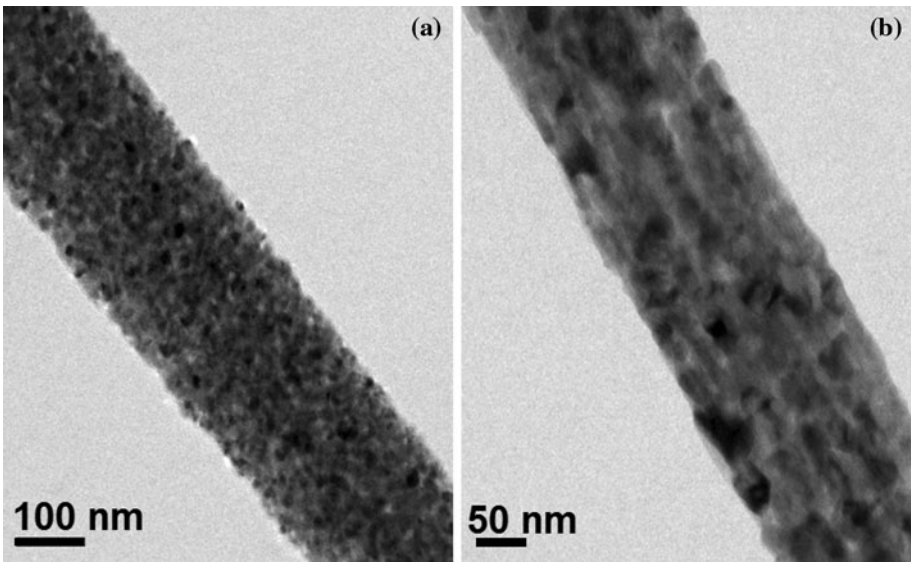

Fig. 13 TEM images of the TiO_2 NFs sintered at 500 °C for **a** 1 h and **b** 24 h. The figures are from those authors' study and reproduced from J Phys Chem C 113:21538, 2009 with permission

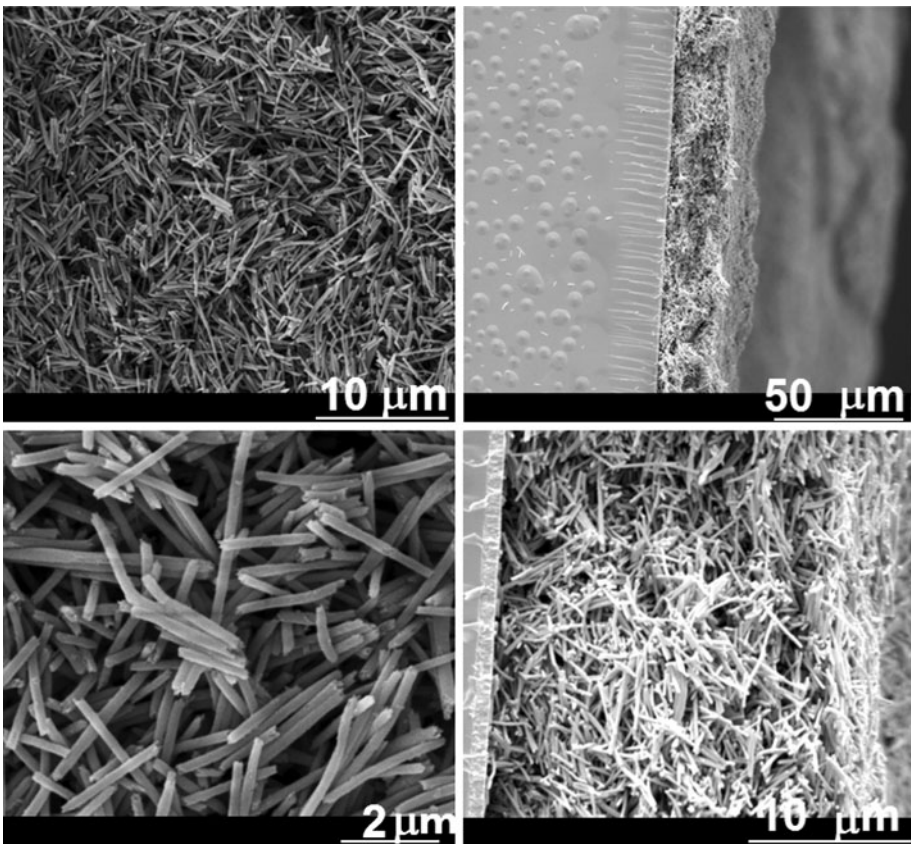

Fig. 14 SEM images of the NWs obtained by ultrasonically dispersing the TiO_2 NFs in acetic acid for 30 min when thick films developed using the NW paste [67] (*top panel*). *Bottom panel* displays the magnified images of the corresponding samples. The figures were from those authors' study and reproduced from J Phys Chem C 113:21538, 2009 with permission

[67] were several orders of magnitude higher than those determined for conventional nanoparticles [79].

Figure 15 shows the OCVD curves displaying the electron lifetime as a function of V_{OC} for 1-h and 24-h heated samples. Shape of the OCVD curve for 1-h heated sample shows a dependence on the quasi-Fermi level confirming a trap-assisted conduction mechanism similar to those of nanoparticles. Similar OCVD was reported for E-spun continuous NFs directly spun on FTO followed by annealing for 1 h [41]. The depression seen in the curve at around 0.3 V indicates the presence of surface trap states that could result in recombination of electrons with the

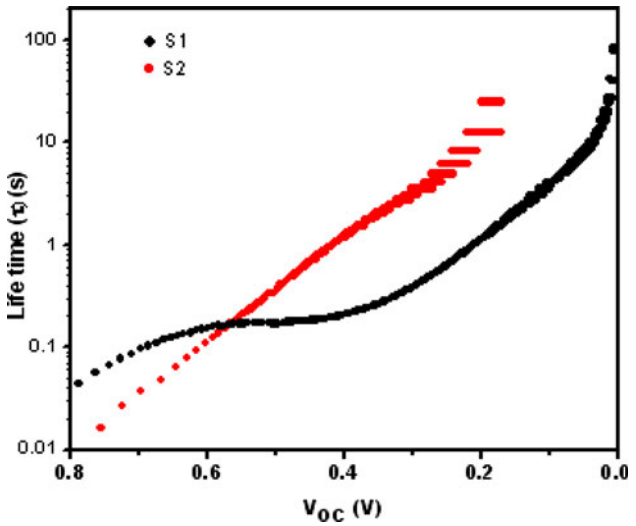

Fig. 15 The OCVD curve measured for the samples heated for 1 h (*black dots*) and 24 h (*red dots*). The figures were from those authors' study and reproduced from J Phys Chem C 113:21538, 2009 with permission

electrolyte through tunneling. Furthermore, the strength of deviation from linear mode suggests a high rate constant for such recombination. Interestingly, the dependence of lifetime on V_{OC} of 24-h heated samples was found to be linear indicating the removal of the surface traps. The DSCs with $\eta \sim 5.8\%$ were reported using ex-situ-annealed samples [60].

The above mentioned efforts on fabricating E-spun TiO_2 NF/wire/rod DSCs require the use of an adhesion layer, hot-pressing, and $TiCl_4$ treatments to realize high efficiencies. We have developed a simple procedure based on a Pechini-type sol of E-spun TiO_2 NRs to realize high efficiency in the DSCs without the need for the above mentioned steps [80]. The E-spun fibers were ground to NRs and mixed with a suitable amount of polyester, and sonicated for ~ 12 h. The side carboxylic acid groups of the polyester would chemically bind to the TiO_2 surfaces which results in a Pechini-type sol ideal for doctor blading. The sol was doctor-bladed to a thickness of ~ 15 μm on an FTO and annealed at 450 °C for 1 h, when the polymer evaporated giving a highly porous (high inner porosity) NRs network ideal for excellent anchoring of the sensitizer. The best DSCs fabricated on an area of 0.28 cm^2 by the methodology gave $\eta \sim 4.3\%$, and an incident photon-to-electron conversion efficiency (IPCE) of 50%. Details of the charge transport mechanism analyzed through impedance measurements showed a lower charge transport resistance (0.81 V), and hence, a good fill factor (62%). More studies on increasing the specific surface area while keeping the higher charge transport properties of the ex-situ-annealed NRs and NWs are currently underway at our laboratory.

Photovoltaic fibers by electrospinning—solar cloths

Development of DSC and polymer-based photovoltaic fibers (PVFs) is a challenging research topic of current interest as these find extensive applications in smart textiles, medical field, sensors industries, etc. Powering wearable and implantable electronic devices in fabrics and sensors is still a daunting task. Several research efforts were directed toward the development of PVFs. Photoelectric response of E-spun NFs consisting of TiO_2 nanoparticles, phthalocyanine, N3, Azo, and Congo red dyes in polyacrylonitrile matrix was reported by Senecal et al. [81, 82]. The E-spun membranes with the azo dye and Congo red showed photoelectric response with the short-circuit current of the order of several nA/cm^2.

We propose that the use of 1D NWs in place of nanoparticles would enhance the photoconversion efficiency. Efficiency of photovoltaic conversion depends on the degree to which the two species, i.e., dye-anchored semiconductor and the polymeric hole-conductor, form a percolating network in addition to the efficiency of charge transport and collection. Figure 16 shows a schematic of this concept.

Owing to their large aspect ratio, NWs are expected to have better connectivity and percolation behavior; and

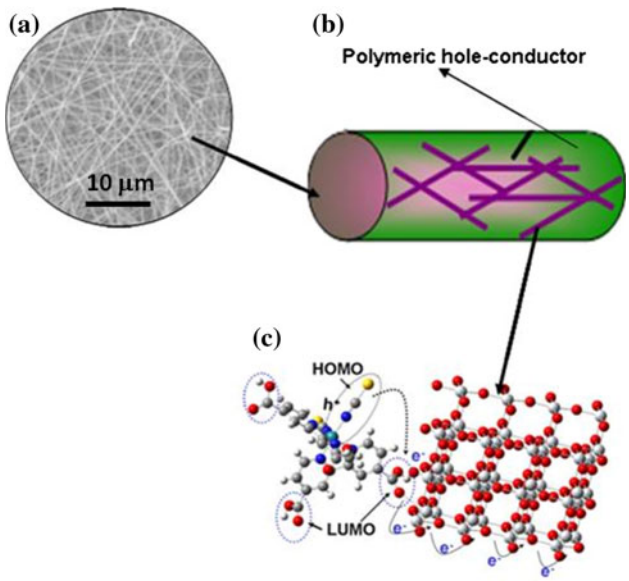

Fig. 16 Concept of photovoltaic fibers. The PVFs are visualized as a non-woven fiber cloth (**a**). The fiber is a percolating network of 1D nanostructures such as nanowires in a polymeric hole-conducting medium (**b**). Organic flourophores such as dyes or semiconducting quantum dots could be anchored to the nanowires to widen the absorption wavelength window (**c**). Light absorption by the flourophores leads to excitation of electrons to unoccupied molecular orbitals which are then injected to the conduction band of the wide bandgap metal oxide semiconductor; the oxidized flourophores are regenerated by a hole conductor

therefore, NWs were used in this study as electron transport medium. Moreover, NWs have higher electron diffusion coefficients. We note that no photocurrent was observed when dye-anchored nanoparticles were dispersed in a polymeric hole-conducting medium possibly due to the increased percolation threshold of the nanoparticle–polymer system or higher fiber diameters (500 nm–1 μm) observed in this study. Main hurdle in this study was to optimize the electrospinnable solution with the dye-anchored NWs of relatively large diameter and length.

The N3 dye-anchored TiO_2 NWs were dispersed in a polymeric solution containing polyaniline (PANi) and polyethylene oxide (PEO), lithium iodide/iodine (LiI/I_2) PANi/PEO, and polyhexyl thiophene (P3HT). The resulting solutions were E-spun at $\sim$30 kV with solution feed rate of 2 mL/h. Figure 17 shows the TEM images of the NFs developed by E-spinning the above solutions. Images a and b show a large area and magnified images, respectively, of the fiber cloths from PANi/PEO/LiI/I_2 and c and d are the corresponding images from PANi/PEO/P3HT system. Beads were observed in the SEM images; however, the fibers were continuous. Possible aggregations in the TiO_2 nanowires could have also increased the bead formation. A closer examination using TEM revealed islands of interconnected TiO_2 nanowires of length $\sim$2 μm dispersed in the polymeric matrix (images e, f). Constraints in the present experiments are the comparatively larger diameter (150 nm) of the starting TiO_2 nanowires likely rendering good percolation among the nanowires difficult. The best one of the PVFs fabricated by this methodology showed an efficiency of $\sim 10^{-3}$%.

One of the factors to be improved for better photovoltaic parameters is to reduce the percolation threshold thereby providing better connectivity with the nanowires. This could be achieved through using long length (4–10 μm) and lower diameter ($\leq$50 nm) nanowires in the hole-conducting polymeric matrix. Other possible ways to improve the efficiency should be to use highly conducting polymers for hole/electron transport. These efforts are currently underway at our laboratory.

Energy storage—lithium ion batteries

As stated before, the renewable energy comes with a dual topic of energy conversion and storage. Many electrochemical devices that integrate different energy storage modes have been investigated in recent years for reversible energy storage, a brief account of which is available in recent reviews [83–85]. The intercalation storage of lithium ions is widely used due to its potentially large operational voltage window, high energy density, fast power capability, safety, and long cycle life. Conventional lithium ion battery (LIB) consists of $LiCoO_2$ (cathode), graphite (anode), and a non-aqueous Li-ion-conducting electrolyte. The lithium ion is inserted in the anode from the cathode (intercalation) during the charge cycle and vice versa during the discharge cycle (deintercalation) due to the electrochemical reactions happening at the respective electrodes (Fig. 18). Nanostructured materials come into picture due to their high specific surface area which will enable absoption of the volume changes due to the smaller number of atoms in the nanograins of the electrodes. Also, an increased access of Li to the alloy-forming metal particles and short diffusion path length for Li ions will enable improved electrode kinetics, solid electrolyte interphase formation, and current-rate capability [86].

Electrospun polymeric membranes for ion transport

The first reports on the use of E-spun fibers [poly(vinylidenefluoride), PVDF] were on their use as membranes for ion transport or as separators [87, 88]. The membranes exhibited a high uptake of the electrolyte solution (320–350%) and a high ionic conductivity at room temperature ($\sim 10^3$ S/cm). A decrease in the fiber diameter constituting the membranes led to an increase in the conductivity due to the high electrolyte uptake. Interestingly, the fibrous polymer electrolyte that contained a 1 M LiPF6-EC/DMC/DEC (1/1/1 by weight) solution showed a high electrochemical stability of above 5.0 V, which increased with the decrease in the fiber diameters. The interfacial resistance (R-i) between the polymer electrolyte and the lithium electrode slightly increased with the storage time, compared with the higher increase in the interfacial resistance of other gel polymer electrolytes. The prototype cell showed stable charge–discharge behavior with minimal capacity loss under constant current and voltage conditions. Later improved performances were observed in poly(vinylidenefluoride–co-hexafluoropropylene) (PVDF–HFP) membranes [89].

Electrospun cathode materials—$LiCoO_2$

The E-spun $LiCoO_2$ NFs were evaluated for LIB electrochemical cycling in 2005 [90]. The cyclic voltammogram curves indicated faster diffusion and migration of Li^+ cations in the nanostructured $LiCoO_2$ fiber electrode [90–93]. In the first charge–discharge process, the $LiCoO_2$ fibers showed the initial charge and discharge capacities of 216 and 182 (mA h)/g, respectively. After the 20th cycle, the discharge capacity decreased to 123 (mA h)/g. A comprehensive study on the dependence of crystallinity and surface area on the specific capacity and cycling stability is still lacking.

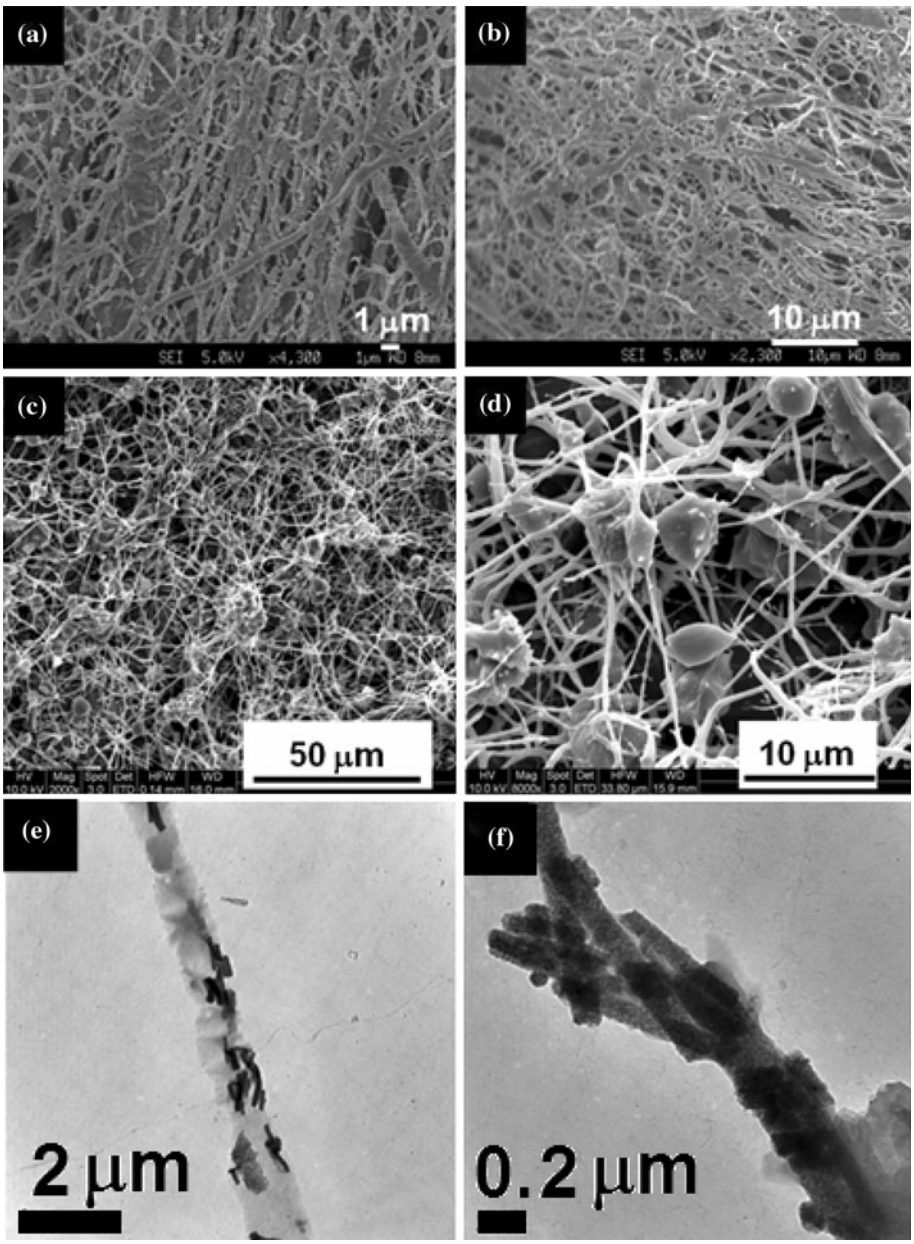

Fig. 17 **a**, **b**, **c**, and **d** are the SEM and **e** and **f** are the TEM images of the photovoltaic fibers (PVFs) developed by electrospinning. The SEM images were measured using a FESEM (Quanta 200 FEG System: FEI Company, USA) and the TEM images by JEOL 2010Fas

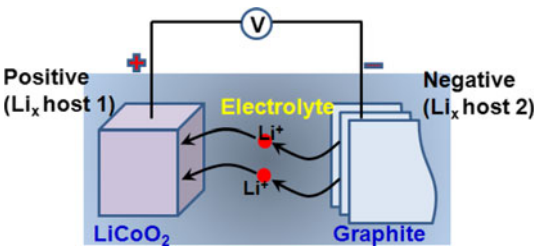

Fig. 18 Structure of the lithium ion battery. The electrochemical reaction at the cathode during charging cycle is $LiCoO_2 \rightarrow Li_{1-x}CoO_2 + xLi^+ + xe^-$ and that at the anode is $xLi^+ + xe^- \rightarrow Li_xC$ (Graphite). The overall reaction during the charging cycle could be written as $LiCoO_2 + C \rightarrow Li_{1-x}CoO_2 + Li_xC$. A reverse reaction occurs during the discharge cycle

Electrospun anode materials

The E-spun carbon fibers and their composites were tested as anodes in the place of conventional graphite [94–97] in the LIBs. Resultant electrodes were mechanically tough due to random web structure; a large accessible surface area due to nanometer-sized diameters; and relatively good electrical conductivity due to 1D fiber morphology. These parameters make it possible to improve the rate capability of LIBs. These studies reached a conclusion that the constant and slightly inclined charge potentials, high reversible capacity, and enhanced cycling at high rate capabilities of the E-spun carbon fiber make them

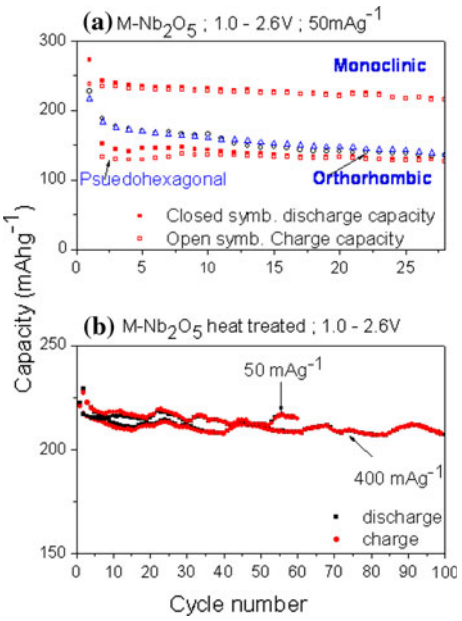

Fig. 19 Capacity versus cycle number plots of **a** bare H, O, and M-Nb_2O_5; current rate: 50 mAg^{-1}. **b** M-Nb_2O_5 heat-treated electrode at 220 °C at 6 h in Ar; current rate: 50 and 400 mAg^{-1}. Voltage range: 1.0–2.6 V, Li-metal as counter and reference electrode [100, 101]

ideal candidates to be employed as anodes for high-power LIBs.

More recently, E-spun metal oxide anodes such as V_2O_5 [98], MnO_x [99], TiO_2 [54, 55], Nb_2O_5 [100, 101], and Co_3O_4 [102, 103] were used as anodes for the LIB. The specific capacity and cycling stability of the resultant LIB depends on the crystallinity and surface area of the respective anode materials (Fig. 19). Incomplete phase formation or highly defective crystalline structure adversely affected lithium intercalation/de-intercalation behaviors both in terms of specific capacity and cycling stability. The peculiar porous structure of E-spun NFs could be beneficial for the observed cycling stability of the LIB which favors a complete desorption of lithium ions during the discharge cycle.

Summary

In order to summarize, significant achievements are made in synthesizing metal oxide NFs with controllable diameter, crystallinity, and surface area. The case of TiO_2 NFs is presented here as a typical example. The TiO_2 NFs with diameter as low as ~20 nm and surface area as high as 200 m^2/g have been synthesized. The DSCs with efficiency as high as 11% has been reported using E-spun TiO_2 NRs through a simple configuration relative to that achieved using mesoporous nanoparticles. The charge transport measurements determined in the presence of an electrolyte using electrochemical impedance spectroscopy as well as transient photocurrent measurements showed that the charge transport resistance through the NFs is much lesser than that due to the nanoparticles, and this property could be exploited to determine a suitable aspect ratio for giving efficient electron diffusion coefficient. Further, it has been shown that the electron diffusion through the NFs could be controlled by tailoring the crystallinity. When dye-anchored wires are dispersed in a polymeric hole-conducting medium and the resultant solution is E-spun to produce a non-woven fiber mat, it could act as a PVF. Some preliminary results were generated at our laboratory. Furthermore, E-spun metal oxide NFs could be efficiently used for electrochemical storage of energy. The LIBs, fabricated using metal oxide NFs as electrodes or polymeric membranes as ion-conducting channels, demonstrated higher operational stability. Since the E-spinning process has the potential to fabricate metal oxide NFs, with superior crystallinity and surface properties and the remarkable properties of the fibers thereby produced, this process, i.e., E-spinning, promises to be a candidate process for material fabrication for future electronic and energy industry.

Nanofibers for water filtration

Fresh water scarcity is a major problem in different parts of the world. Many technologies are widely employed to get usable water from brackish, waste, and salt water. Traditional approaches like distillation, sand filtration, sedimentation, and treatment with chlorine are widely used [104]. Filtration using membrane technology is a relatively new [105] with advantages over traditional water purification methods such as scalability, low power consumption, and the non-usage of chemicals. Inevitably, membranes can be operated at ambient temperatures which are favorable for biological, drug, and food applications [106]. In general, membrane acts as a very specific filter that will pass water flow through, while it separates suspended solids and other substances.

Membrane filtration can be broadly divided into two parts based on the particle sizes filtered: micro and ultra filtration for the removal of larger particles as membranes operate at low pressures with high productivity. On the other hand, nano filtration and reverse osmosis (RO) remove salts from water. In nano and RO membranes, separation takes place mainly by diffusion through the membrane and not by the principle of pores. The pressure required to operate nano filtration and RO is much higher than that required for micro and ultra filtration, while productivity is much lower. Figure 20 shows a schematic of membrane filtration processes.

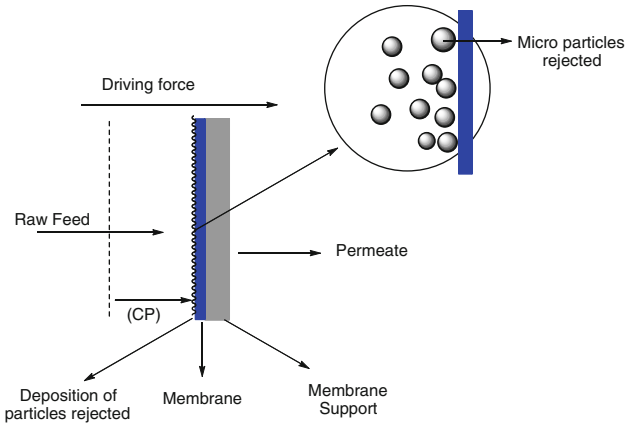

Fig. 20 Schematic diagram of membrane filtration process depicting various fouling methods: concentration polarization (CP), deposition of particles rejected on the feed side, fouling of the membrane on the skin void space

However, main disadvantages of the membrane materials are fouling which forms quickly when exposed to the organic species in waste water feed streams. The main method of preventing membrane fouling includes surface grafting of hydrophilic polymers onto the membranes. The former approach works fairly well, but it requires a modified number of fabrication steps and the surface treatments tend to lose their membrane strength.

Membranes and materials

Filtration is a process of removing suspended particulates from water by applying pressure to drive the water through a porous media. With the proven success of membranes in the water filtration media, membrane technology continues to make advancement. Even though advanced membranes are developed, major problems still needing attention are the membrane fouling and chemical stability. Reduced fouling would make membranes become cost effective by extending their operational lifetime and lowering energy requirements. The size of particles removed and permeated by the types of membranes are summarized in Table 2.

Most of the microfiltration (MF), ultrafiltration (UF), nanofiltration, and RO membranes are synthetic organic polymers, although other forms of membranes including ceramic and metallic are available. Currently, almost all the membranes manufactured for drinking water production are made of polymeric material, since they are significantly less expensive than membranes constructed of other materials. MF and UF membranes are often prepared from same materials, under different membrane formation conditions so that different pore sizes are produced [107]. The polymers for MF and UF include polysulfone, poly(acrylonitrile), poly(vinylidene fluoride), poly(acrylonitrile)-poly(vinyl chloride) copolymers [108] and poly (ether sulfone). The MF membranes also include cellulose acetate–cellulose nitrate blends, nylons, and poly (tetrafluoroethylene). The RO membranes are typically made up of either cellulose acetate or polysulfone coated with aromatic polyamides [108]. The NF membranes are made from cellulose acetate blends or polyamide composites like the RO membranes.

Methodology

E-spinning [109] is one of the most effective and versatile method to produce polymer NFs [5, 110–113]. E-spinning is a fiber-forming process that utilizes a high-voltage electric field to produce an electrically charged jet of polymer fluid, which, while solidifying, produces a fibrous web comprising fibers from a few nanometers to submicron in diameter. E-spun NFs were successfully used as high performance filters for air filtration [114] and also in protective textiles [115–117], advanced composites [118–120], photovoltaic cells [81], scaffolds in tissue engineering [121–125], solar cells in space [126], and recently as membranes in affinity separation [127].

Our research group has extensively studied the impact and application of E-spun nanofibrous membranes for various separation technologies. Investigations have revealed E-spun nanofibrous membranes (ENMs) possess high-flux rates and low trans-membrane pressure [128]. These characteristics are due to (a) high porosity, (b) interconnected open pore structure, and (c) tailorable membrane thickness. In general, membrane processes operate in two modes: dead-end or cross-flow methods as shown in (Fig. 21). In dead end flow, the feed is forced through the membrane, increasing concentration of the rejected components in the feed. In cross flow, the

Table 2 Summary of different membrane processes

	Microfiltration	Ultrafiltration	Nanofiltration	Reverse osmosis
Type of particles removed	Colloids bacteria	Large organic molecules, viruses	Small organic molecules, divalent ions	All dissolved species
Operating pressure (bar)	0.2–2	1–5	5–20	20–80
Typical flux (l/m^2/h)	100–1,000	50–200	20–50	10–50

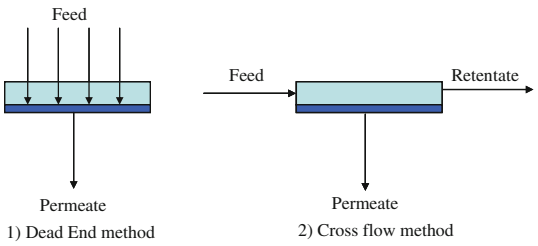

Fig. 21 Schematic representation of modes of flow

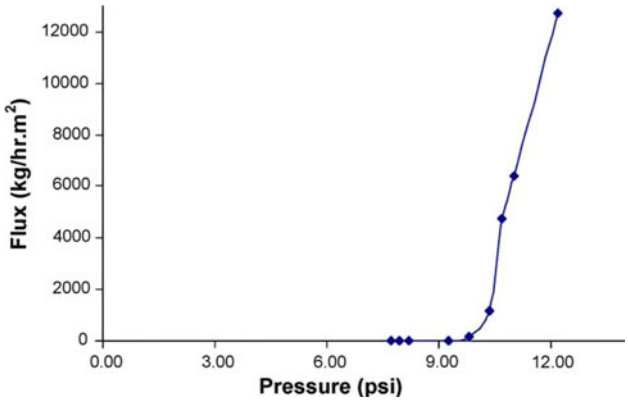

Fig. 22 Pressure versus flux for E-spun (PVDF) membrane [128]

occurrence of concentration polarization and fouling of the membrane is reduced.

Using the developed ENMs, the liquid entry pressure of water was determined using pore size measurement set-up, which indicates that beyond the upper pressure limit, the flux is directly related to pressure (Fig. 22).

Later, the developed ENMs were subjected to micro particle separation using polystyrene micro particles at different concentration. A comparison of the results shows that the developed ENMs have characteristics similar to that of the MF membranes (Table 3).

The chemical and physical properties of the membrane's surface play an important role in determining the flux and selectivity of a separation process. Hence, surface modification is a powerful tool in membrane technology, which can be used to enhance the performance of membranes. Polymers suited for membrane applications should preferably be chemically stable and mechanically strong. Traditionally, polymers with the best solvent resistance or those which provide the most convenient pore structure should be too hydrophobic for use as a filter in aqueous media [129]. Conversely, polymers with the desired active surfaces do not possess adequate mechanical stability, and hence, cannot be used as a support or base membrane [130]. Thus, surface modification is frequently employed to combine the attributes of a desirable surface chemistry and adequate mechanical stability.

Blending, interfacial polymerization, grafting, and surface coating are the various methods available for surface modification. Among these, plasma-induced graft copolymerization is an efficient and versatile method for introducing a selective polymeric layer on the surface of a hydrophobic membrane. The surface pores of the ENMs can be reduced significantly by plasma-induced grafting, without compromising on its bulk porosity. The thickness of the modified layer can be controlled up to the angstrom level [131].

Kaur et al. [132] utilized plasma-induced grafting to reduce the surface pores of the ENMs while maintaining the base nanofiber architecture. This modification technique created an asymmetric membrane structure. Various grafting techniques had also been employed to impart specific surface chemistry on the fiber surface. The commonly available PVDF and PSU polymers were electrospun, and these ENMs were exposed to plasma at different power and exposure time. Further, polymerization was carried out at certain temperature in monomer solution such as methacrylic acid (MAA) for a specified time to create the high performance UF membrane [132]. This study evaluated the application of plasma-induced graft copolymerization to reduce the surface pores of ENMs.

The available polymer poly(vinylidene) fluoride (PVDF) was E-spun as the base membrane, and a hydrophilic monomer methacrylic acid (MAA) was grafted on the surface of the ENM to develop an asymmetric membrane with enhanced flux performance. Concomitantly, grafting was performed on a commercial phase-inverse PVDF (HVLP) membrane, and membrane performance of the

Table 3 Separation results of 1-, 5-, and 10-μm polystyrene micro particles using ENM

Particle size (μm)	Membrane area ($\times 10^{-4} m^2$)	Pressure (psi)	Feed (ppm)	Water flux start of expt (kg/m^2h)	Feed flux (kg/h)	Water flux end of expt (kg/h)	Separation factor (%)
10	3	8.3		133	133	133	96
1	3	8.3	500	200	200–133	200	91
1	3	8.3	–	467	Drop in flux	–	–
1	3	9.5	100	1300	1066–530	530	98

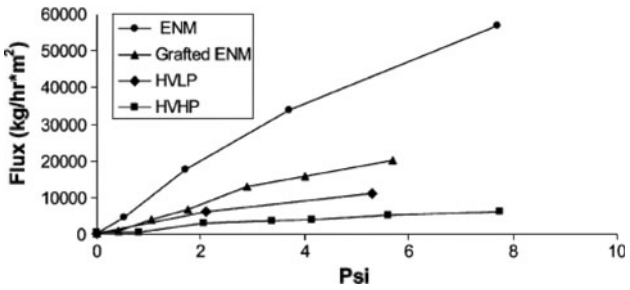

Fig. 23 Water flux permeation results of ENM, grafted ENM, HVLP, and HVHP [132]

ENM with the grafted layer was compared with the commercial membranes. More significantly, water filtration results revealed that the grafted ENM had a better flux throughput than the HVLP membrane, which proved that ENMs were successfully engineered through surface modification to achieve smaller pores while retaining their high flux performance (Fig. 23).

In order to further advance the role of ENMs in liquid separation, several approaches to introduce a polyamide layer on the surface of the ENM through interfacial polymerization to develop membranes suitable for nanofiltration. The nanofiltration (NF) membrane is a type of pressure-driven membrane with properties in between RO and UF membranes. NF offers several advantages such as low operation pressure, high flux, high retention of multivalent anion salts, relatively low investment and low operation and maintenance costs. Because of these advantages, the applications of NF worldwide have increased.

Very recently, Kaur et al. [133] fabricated polyamide composite membranes based on an E-spun porous nonwoven support. Through surface modification, these membranes could be used beyond the microfiltration range. A polyamide layer was introduced on the surface of the porous E-spun NF membrane through interfacial polymerization. Different approaches to facilitate the formation of the thin film on the ENMs have been systematically explored and interesting surface morphologies have been summarized. Owing to extreme hydrophobic nature of PVDF base membrane, common practice of soaking the membrane in an aqueous phase followed by organic phase were reversed, which paved the way for the best separation results.

E-spun PVDF polymeric fiber membranes in two different concentrations were developed. The membranes were heated from room temperature to 60 °C for 1 h at a rate of 1 °C/min to ensure complete removal of adhered organic solvents such as acetone. Subsequently, the membranes were then heated up to 157 °C/min at the same rate for 3 h to improve the structural integrity of the membrane. A polyamide thin film layer was formed through interfacial polymerization reaction of p-phenylenediamine (PPD)/aqueous phase and trimesoyl chloride (TMC)/organic phase.

The membranes were characterized for morphology and pore distributions. The surface and the cross-section of the membranes were observed by FESEM. The pore size distribution of the support membrane was evaluated using a capillary flow poromoter (Porous Materials Inc., USA). Circular composite ENM 25 mm in diameter were used for flux and separation studies All the tests were conducted on Amicon-stirred cell model 8010 at an operating condition of 70 psi.

The best interfacial polymerization condition performed on the surface of the ENM resulted in the rejection of 80.7% of $MgSO_4$ and 60% of NaCl (Table 4).

Using the modified approach, a polyamide thin film was successfully produced (Fig. 24). The ratio of monomers played an important role in the rejection of the salts, and by varying the ratio between two monomers, the rejection of the salts was increased. The preliminary results proved the potential of ENM as self-supporting nanofilters. However, with careful optimization of the surface film, the flux may be greatly improved. With better optimization and understanding of their separation behavior, efficient nano-filters based on E-spun membranes can be designed and developed.

Summary

In order to summarize, E-spun NFs have high potential in the improvement of water filtration membranes. Fouling of membranes by organic micro pollutants, heavy metals, pharmaceutical and personal care products, and biofouling of membranes caused by the bacterial incumbrance in

Table 4 Flux and separation profile of the ENM-based composite membranes

Ratio of TMC conc: PPD concentration	$MgSO_4$ experiment[a]		NaCl experiment[a]	
	Rejection (%)	Flux (L/m^{2}h)	Rejection (%)	Flux (L/m^{2}h)
1:1	0	–	0	–
1:2	42.0	1.24	42.5	1.2
1:4	75.3	0.66	61.6	0.56
1:16	80.7	0.51	67	0.52

[a] Solute concentration in feed 2000 ppm, operation pressure 70 psi

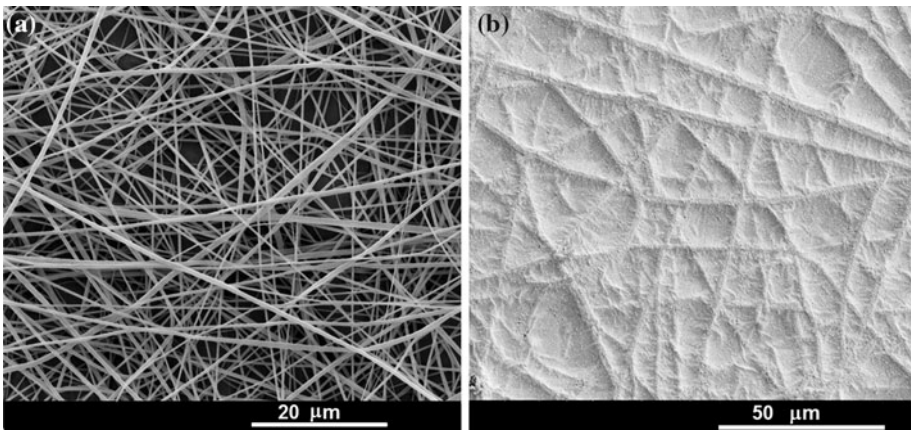

Fig. 24 **a** Structural architecture of PVDF ENM. **b** Polyamide thin film on the surface of ENM

water reduce the quality of drinking water and has become a major problem in water treatment. Several studies showed inhibition of these bacteria to reduce the fouling/biofouling after exposure to NFs with functionalized surfaces. As the sustainability of drinking water availability is challenged worldwide, nanofiltration is becoming one of the most important technologies in this century for water treatment due to its superb efficacy in producing a high quality of water at relatively low costs. By E-spinning, ultrafine fibers were created from various polymers and other materials, with diameters ranging from a few μm down to tens of nm. The nonwoven webs of fibers formed through this process typically have nano-scale pore sizes, high and controllable porosity, high specific surface areas, and extreme flexibility with regard to the materials used. Surface chemistry of the E-spun NFs could be modified by blending, grafting, coating, and interfacial polymerization. Finally, future research with E-spun NF membranes could pursue new pretreatment technologies that can improve the quality of treated water and, more importantly, can control membrane fouling in a cost-effective and environmental-friendly manner.

Nanofibers for regenerative medicine

Before the turn of this century, E-spinning had only been used commercially in air filtration, and not much attention was paid to it in the research community. In the mid-1990s, interests in nanotechnology and tissue engineering have caught the attention of researchers. For the first time, a scaffold that has the same nano-building blocks of extracellular matrix (ECM) can be fabricated easily. The NFs have been shown to yield cellular response that differs from that of traditional smooth-surfaced substrate. Advances in E-spinning have allowed construction of NF scaffolds, which mimics more complex micro-structural arrangement of certain ECMs. Bone, nerve, and cardiac regenerative scaffold will be described here to illustrate the advancement of biomimetic scaffolds. Taking into account the benefits of NFs in tissue regeneration, NFs can be applied to existing biomedical devices. An illustration of this capability will be shown using NF-coated stent as an example.

Advantage of E-spun fibers

Common materials that have been E-spun for biomedical applications include biodegradable synthetic polymers, such as polylactic acid, polycaprolactone, and polyglycolic acid, and non-biodegradable materials such as polyurethane, and natural polymers such as chitosan, collagen, and alginate. Therefore, specific material can be chosen based on the criteria that match the requirement of scaffold. However, in certain biodegradable materials, the property of the material may differ from the bulk property and must be verified at nanometer scale. For example, polylactic acid NF does not undergo accelerated catalytic hydrolysis which is commonly seen in bulk polylactic acid [134]. This may result in less severe reaction in the tissue from the degraded PLA product due to slower degradation rate.

Mimicking ECM has been one of the main motivations for exploring its use as tissue regenerative scaffolds (Fig. 25). Till date, many different cell lineages and stem

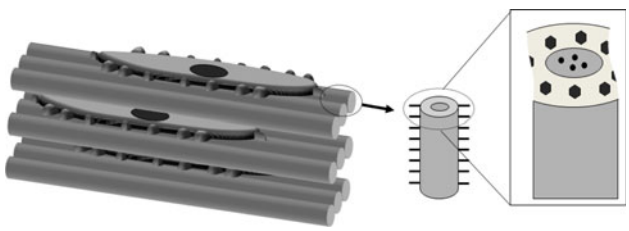

Fig. 25 Motivation of using E-spun NFs for tissue engineering. Functionalized hierarchically organized nanofibrous scaffold has the potential to enhance cell adhesion, promote cell proliferation, and differentiation as well as migration and physical morphology

cells have been cultured on E-spun NFs and have yielded fair to excellent results. In terminally differentiated cells such as smooth muscle cells, osteoblast, chondrocytes, cardiomyocytes, and endothelial cells, the E-spun NFs have been demonstrated to show enhanced proliferation and adhesion [135]. Gene expression studies on endothelial cells cultured on NFs showed upregulated expression of ICAM-1, VCAM-1, and E-selectin compared to cells cultured on tissue culture plates [136]. Nur-E-Kamal et al. showed that fibroblast and rat kidney cells cultured on NFs resulted in the activation of GTPase Rac which is vital in normal cellular activity in contrast to higher level of Rho kinase released by cells cultured on 2D surfaces [137]. Mechanical stimulation of rat skeletal myoblasts cultured on NF scaffold and 2D film showed earlier and higher expression of integrin $\beta 1$ and integrin-linked kinase (ILK) level for cells cultured on NFs [138]. Stromal cells, such as mesenchymal stem cells [139, 140], haemopoetic stem cells [141], embryonic stem cells [142], and neural progenitor cells [143] have been cultured on NFs. Li et al. have shown that human mesenchymal stem cells cultured on NF scaffold can be induced to differentiate along adipogenic, chondrogenic, or osteogenic lineages by culturing in specific differentiation media [140]. Prabhakaran et al. showed that mesenchymal stem cells cultured on NFs can be induced to differentiate into neuronal cells in neuronal-inducing factors.

Contact guidance of cell migration and proliferation has been demonstrated using various aligned nanostructures. Cell organization in ECM is also influenced by its underlying ECM organization. Through modification of the E-spinning setup, scaffold consisting of aligned NFs can be fabricated, and this has been shown to influence cell behavior. In vitro culture of dorsal root ganglia by Corey et al. has shown that neurites' outgrowth on highly aligned substrate were 20% longer than that of neurites on randomly oriented NFs [144]. Chew et al. showed that human Schwann cells had not only aligned to the orientation of NF, but also shown upregulation of the myelin-specific gene, P0, which was absent in randomly oriented NFs [145]. Other cells such as endothelial cells, smooth muscle cells and fibroblast have been shown to orient in the direction of the underlying aligned NF direction [123, 146, 147].

Mimicking ECM chemical composition

Although ECM was previously thought to give just structural support to cells, it is now recognized that integrins on ECM and cytokines bound to ECM are able to interact and influence cell behavior. Therefore, just mimicking the physical structure of ECM may not be sufficient. Chemical composition and addition of proteins are sometimes necessary to regulate cell behavior. Studies have shown that cells have better adhesion and proliferation on the NFs containing proteins than the purely synthetic NFs [136].

Since the addition of biochemical cues have a positive influence on cell behavior, various methods have been explored for this purpose. Polymer solution blending has proven to be one of the most commonly used methods, as it does not require any additional setup or equipment. In this technique, only one of the materials needs to be E-spinnable, and the others can be small biological molecules and fragments. Proteins, such as fibrin [148] and collagen [121], DNA [149], virus [150], and GAG [151], have been successfully mixed and E-spun to give functional NFs. Although a common solvent is not required, the distribution of the two components in the fluid should be uniform. Another common technique is through surface modification, where biological entity is attached only to the surface of NFs. An advantage of this technique is that, usually, a small amount of biological cue is required to evoke a desirable response from the cells. Surface modification can be achieved through plasma treatment on the NF surface and dipping NF into a solution containing the biomolecules [152]. More elaborate setup such as using core–shell spinneret to generate core–shell NFs has also been used. In this case, the spinneret contains a dual bore where the inner solution is usually different from the outer solution. With this, solvent-sensitive biomolecules can be incorporated through the inner core using water, while the outer shell may use solvent-based polymer.

Native bone is known to contain up to 70% nanohydroxyapatite (nHA) with the rest consisting predominantly of collagen NFs. Therefore, in the construction of a biomimetic regenerative bone scaffold, it is important to incorporate hydroxyapatite. Studies have shown that the presence of hydroxyapatite stimulates secretion of bone-like minerals by osteoblasts on NF scaffold compared to those without nHA [153]. While blending would incorporate nHA in the NF matrix, other mineralization technique has been successful in introducing nHA on the surface. Simulated body fluid has been shown to deposit nHA on the surface of NFs after a week or two of immersion [154]. Ngiam et al. used the alternate dipping method, where the NFs were first dipped in calcium solution followed by phosphate solution, to form nHA on the NF surface in a few hours [155].

Mimicking ECM hierarchical structure

Many biological structures are built in a hierarchical manner with nanostructures coming together to give microstructures which are then organized to a macro-scale level. Researches have shown that nanotopography is able to influence cell functions. Therefore, in the construction of

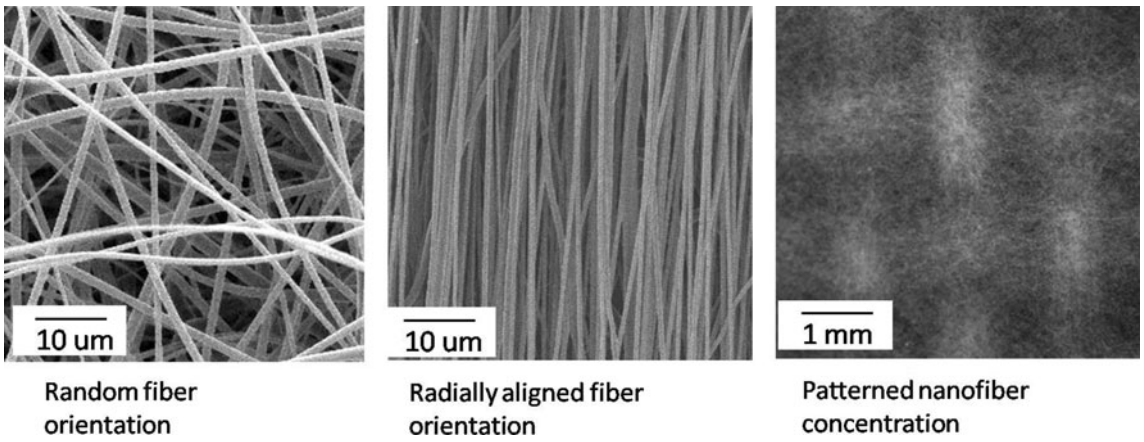

Fig. 26 Nanofiber organization in membrane

regenerative graft, it is important to consider incorporation of nanoscale surface features. Nanoscale topographic modification of dental and orthopedic implants has shown great promises in clinical applications [156, 157]. However, the ideal scaffold should replicate the nano to microscale organization in native ECM.

Progress in the E-spinning process has allowed us to replicate some of the simpler structural organization from the nanoscale. The chaotic jet which is intrinsic to E-spinning generally yields a nonwoven mesh of NFs. Over the last decade, more innovative setups and configurations have led to an evolution in the NF architectures and applications. Figure 26 shows the advancement in nanofibrous membrane organization. At the simplest level of organization, E-spun NF membrane with its nonwoven NF organization resembles connective tissues of ECM. Advantage of aligned NFs in contact guidance of cells has prompted other researchers to develop various methods to fabricate them. Generally, fabricating aligned NF membrane can be achieved through mechanical rotation, air gap between parallel electrodes or their combination. Other researchers have used metal grids to collect E-spun NFs [158, 159], and these materials have been shown to yield better burst strength [158, 159].

While membrane can be used in in vitro cell culture studies and as dermal patch, the NF assembly needs to be modified for it to be used in other regenerative graft application. In vascular graft and peripheral nerve graft, a tubular scaffold is required. Using a rod as a collector during E-spinning has been shown to be a simple method of fabricating tubular NF construct. In the beginning, only randomly oriented NF tubular graft have been used as vascular or nerve graft [160–162]. However, increasing knowledge on mechanical and materials properties have led to the development of multi-layered and multi-functional tubes to mimic the strength and physical structure of blood vessels [163]. Teo et al. have demonstrated the ability to E-spin tubular NF structure with controlled fiber alignment through auxiliary electrodes to guide the flight of E-spinning jet [164]. These properties of the resultant graft can be altered through material selection and NF orientation. Figure 27 shows the advancement in vascular NF graft design. A 12-week study by Nottelet et al. showed that the NF graft implanted in a rat aorta model demonstrated good patency, full endothelialization, and cells' ingrowth [165].

In peripheral nerve graft, biomimicking of the ECM has evolved from just using a conduit with randomly oriented NFs [161, 166] to the inclusion of intra-luminal guidance channel. Native nerve lumen is not an empty conduit-like blood vessel. Instead, it is filled with endoneurium tubes which support the axon and other tissues such as blood vessels and fascicles. As aligned NFs have been shown to guide neurite outgrowth, Chew et al. fabricated a conduit with E-spun fibers aligned along the length of the tube and compared it with circumferentially aligned NF conduits in a rat sciatic nerve model. However, no significant difference in the recovery was found at the end of 3 months although they perform significantly better than empty tube (smooth wall) of the same material [167]. In an effort to mimic the intraluminal support of native nerve ECM, Clements et al. inserted thin film of longitudinally aligned NFs into the lumen of semi-permeable polysulfone tubing. In vivo study using rat sciatic nerve model showed that a single film performs better than 3-film conduit [168]. Where intra-luminal guidance channel is used, there must be a compromise in the number of guidance channel to be inserted versus the blockage of axon growth due to the guidance channel. Figure 28 shows advancement in the nerve NF graft design.

Other than film and tubular structures, NF structures such as yarn and 3D block have been developed. Such structures have the potential to be used in other tissue regenerative graft. In an unpublished study, micro-yarn

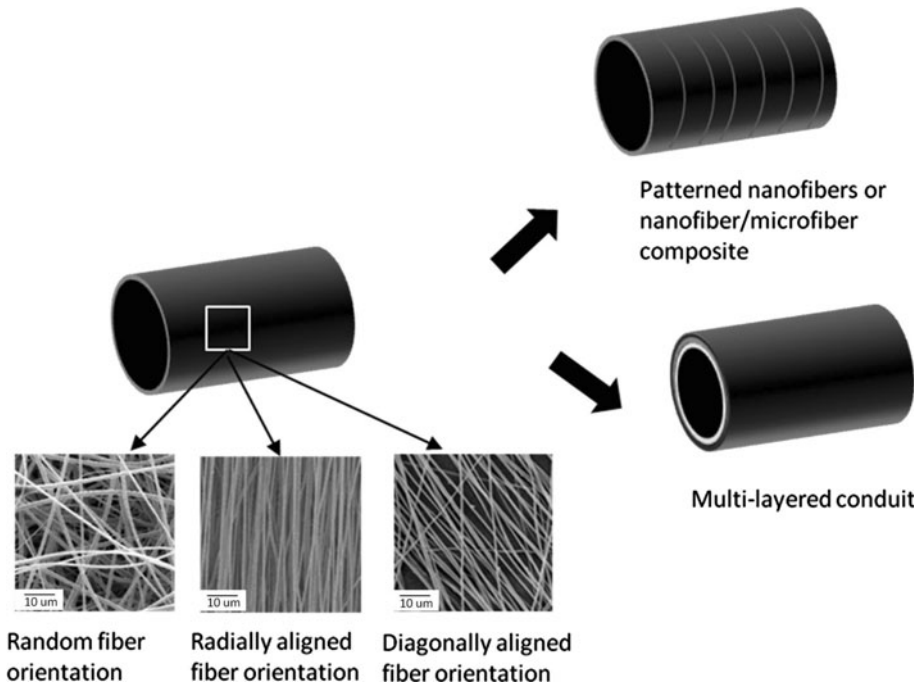

Fig. 27 Advancement in nanofibrous vascular graft

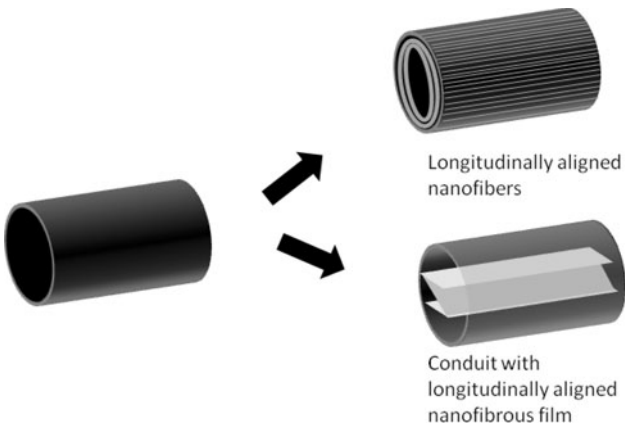

Fig. 28 Advancement in peripheral nerve repair nanofibrous graft

consisting of aligned NFs as shown in Fig. 29 has been used as intra-luminal guidance channel in peripheral nerve repair graft. Various yarn-spinning techniques have been developed; in particular, the technique where E-spun NFs were first deposited onto a non-solvent before drawing into yarn has been highly successful in fabricating aligned NF micro-yarn [169, 170]. The development of process to fabricate 3D block NF's scaffold is a significant development in the use of NFs as regenerative graft. Although in vitro study with NF membrane has demonstrated to encourage cell adhesion and proliferation, many tissues exists as3D block. Therefore, with the process to fabricate3D block NF scaffold, the synthetic graft has the potential to be used in clinical applications. Teo et al. has demonstrated that it is possible to fabricate a hierarchically

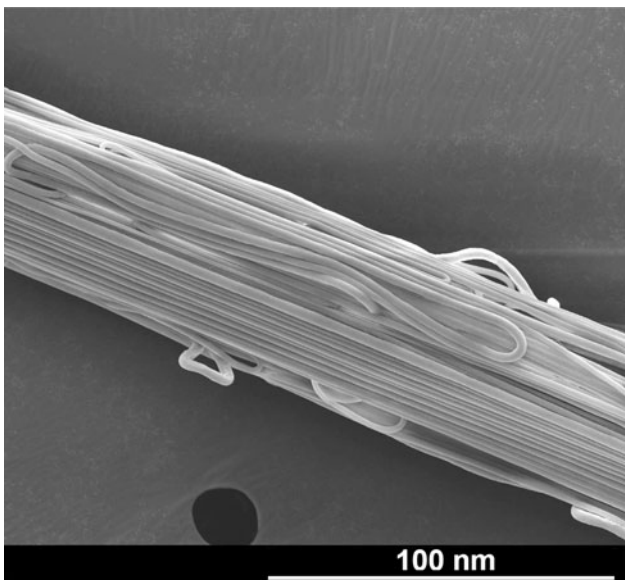

Fig. 29 Aligned nanofibrous yarn

organized block NF scaffold consisting of yarn microstructures [171]. Mineralization technique can be carried out to deposit nano-hydroxyapatite on the scaffold. With this, a hierarchically organized block construct consisting of nano-hydroxyapatite on NFs can be fabricated as shown in Fig. 30.

Medical devices

Currently, most research studies focus on new product development, in particular, regenerative graft. However,

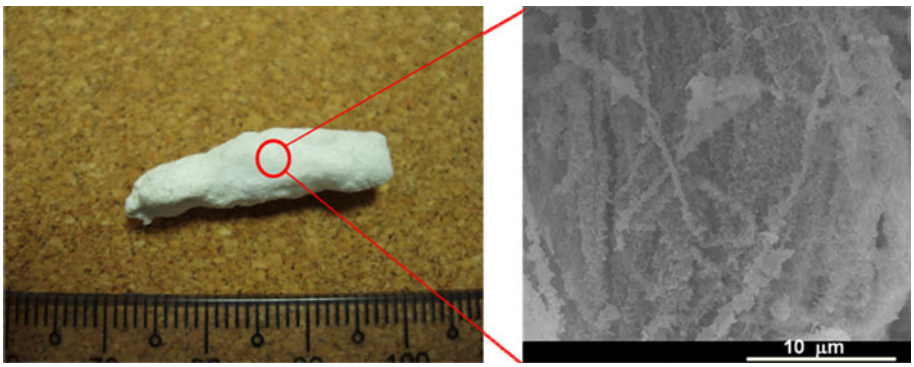

Fig. 30 3D nanofibrous scaffold with nano-hydroxyapatite

E-spinning can also be used to incorporate NFs with existing biomedical devices. Investigation of NFs as vascular conduit has demonstrated that the endothelial cells proliferate well on NF surface. This beneficial effect has been applied to bare metal stent by coating the stent with NFs. Since E-spinning can be used to fabricate NF conduit by coating on a metallic rod, the same method has been used to coat NFs on bare metal stent. Cases of in-stent restenosis due to proliferation of smooth muscle cells into the bare metal stent has prompted the development of covered stent. Covered stent has also found applications in treating aneurysms. Current commercially available covered stent is mainly made out of Teflon which is hydrophobic and discourages endothelial cell proliferation into the lumen of the stent. This poses a risk of thrombosis in the long term as Teflon is non-biodegradable. In contrast, if a layer of endothelial cells are able to cover the lumen of the stent, the risk of in-stent restenosis and thrombosis can be significantly reduced.

Kuraishi et al. carried out an in vivo study of a bare metal stent coated with a layer of randomly oriented NFs in a rabbit aneurysms model. The covered stent was found to be effective in occluding the aneurysms and patent. At day 10, a neointimal layer was formed in the coated stent [172]. In order to reduce the risk of NF coating tear and to minimize the impedance of NF-coating on the stent during expansion, longitudinally aligned NFs can be deposited on the NFs. This will allow stiffer biodegradable polymers to be used for stent coating. Figure 31 shows the bare metal stent coated with polylactide-co-ε-caprolactone NF which has been expanded.

Cardiac tissue engineering

Heart failure following myocardial infarction continues to be the leading causes of death in the United States and industrialized countries. The critical cause of heart failure is myocardial ischemia, resulting in dysfunction and death of cardiomyocytes. The main cardiac response to myocardial infarction (MI) can be seen as cardiomyocyte hypertrophy, apoptotic myocyte loss, progressive collagen replacement, and enlargement of the left ventricle [173]. The cardiomyocytes are starved of oxygen, and nutrients undergo necrosis and apoptosis leading to MI. Cardiomyocytes are essential for the contractile activity of the heart, death of which can eventually lead to congestive heart failure (CHF) and other cardiac dysfunctions [174]. Left ventricular dilatation is a well-recognized precursor of ventricular dysfunction and CHF after myocardial infarction. The damaged left ventricle undergoes progressive "remodeling" and chamber dilation, with myocyte slippage and fibroblast proliferation. The enlargement in ventricular volume leads to progressive structural and functional changes in ventricles (called ventricular

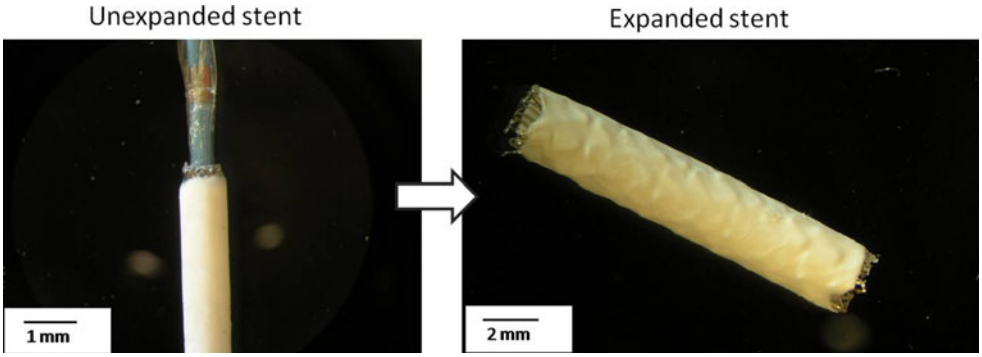

Fig. 31 Nanofiber-coated stent crimped on a balloon (*left*) and an expanded stent (*right*) (Photo courtesy: A. Paneerselvan)

remodeling). Ventricular remodeling is compensatory at the initial stages, but adds further inefficiency to the mechanical pumping of the ventricular muscle, predisposing toward the final stage of CHF, a condition in which the heart cannot pump sufficient amount of blood to meet the metabolic requirements of the body [175]. Restoration of heart function by replacement of diseased myocardium with functional cardiomyocytes is an intriguing strategy because it offers a potential cure. There is an increasing body of experimental approaches to restore/regenerate failing myocardium. Two of the promising pathways are direct implantation of primordial type of cells into the injured heart and the replacement portions of the heart muscle with tissue-engineered bioartificial grafts. Several promising tissues on engineered technologies have already been developed and are presently being tested in animal models, and also in stem cell therapy that has successfully proved in human clinical trials. The ultimate goal in therapeutic cardiac tissue engineering is to generate biocompatible, non-immunogenic heart muscle with morphological and functional properties of natural myocardium.

Cell therapy for myocardial infarction

Cell therapy is a novel treatment to prevent ventricular dilation and cardiac dysfunction in patients suffering from MI. Cell therapy presents new opportunities to enhance cardiac performance through differentiation of injected cells into cardiomyocytes. Although early studies opened the plausibility of cell therapy to regenerate cardiomyocytes, subsequent studies failed to advance through follow-up on these initial observations. Cell transplantation is considered to be a novel and hopeful therapeutic alternative to support endogenous regenerative mechanisms in ischemic heart disease and heart failure. Potential cell sources used for MI include skeletal myoblasts, crude bone marrow, endothelial progenitor cells, hematopoietic stem cells, mesenchymal stem cells, smooth muscle cells, umbilical cord cells, fibroblasts, human embryonic stem cells, fetal cardiomyocytes, and myocardial progenitors. Dib et al. [176] assessed safety and feasibility of using minimally invasive cardiac transcatheter for acute myocardial infarction to previously infarcted myocardium [176]. Autologous myoblast transplantation has the capacity to replace lost myocardial contractile cells [177] plus arrest and reverse ventricular dilation [178]. Opie and Dib [179] observed the improvement in left ventricular ejection fraction (LVEF), wall motion score index, and electrical activity in infarcted myocardium suggesting that the myoblasts remain viable after transplantation for the overall activity of heart function [179]. Mesenchymal stem cells (MSCs) have substantial capacity to facilitate cardiac repair following acute MI, participate in vasculogenesis and angiogenesis by paracrine signaling, incorporation into newly formed vessels, and most likely transdifferentiation into vascular endothelium and smooth muscle cells [180, 181]. Ramakrishna et al. are focusing research on using rat cardiomyocytes and MSCs for the repair of MI (Fig. 32).

Biomaterial scaffolds for cardiac tissue engineering

The challenges in heart muscle tissue engineering include the design and fabrication of noninvasive biomaterial constructs and hydrogels for the regeneration of MI. The criteria and objectives for developing a cardiac patch for cardiac tissue engineering are: (1) it is highly porous with large interconnected pores (to facilitate mass transport), (2) hydrophilic (to enhance cell attachment), (3) structurally stable (to withstand the shearing forces during bioreactor cultivation), (4) degradable (to provide ultimate biocompatibility of the tissue graft), (5) elastic (to enable transmission of contractile forces), and (6) non-immunogenic having the ability to differentiate into mature, functional cardiomyocytes [182]. Scaffold structure determines the transport of nutrients, metabolites, and regulatory molecules to and from the cells, whereas the scaffold chemistry has an important role in cell attachment and differentiation. Mechanical properties of the scaffold should comparably match to those of the native tissue, to provide mechanical integrity of the forming tissue and support an in vivo-like mechanotransduction between cells and their environment. The cardiac tissue constructs express structural and physiological features characteristic of native cardiac muscle have been engineered in vitro using fetal CM on collagen fibers, poly(glycolic acid) fibrous scaffolds, and porous collagen scaffolds. The stress–strain curves of heart muscle and the poly(glycerol sebacate) scaffolds tailored to match either the stiffness of the heart muscle at the beginning of diastole (stiffness is 10–20 kPa) or the stiffness at the end of diastole (200–500 kPa) [183, 184]. The pore size in the range of 50–100 μm was sufficient to allow the vascularization of the scaffold following transplantation. In order to promote functional assembly and electrochemical cell coupling, synchronous contractions of cultured constructs were induced by applying electrical signals designed to mimic those in native heart. Leor et al. (2009) reported cardiac grafts using alginate scaffolds attenuated left ventricular remodeling and heart function deterioration in animal models of myocardial infarction [185]. Jin et al. [186] observed poly(lactide-co-caprolactone) served as a mechanical ECM, allowing the seeded bone marrow MSCs to survive and differentiate into cardiomyocytes, thereby regenerating the myocardium and ultimately ameliorating cardiac function [186]. Zimmermann et al. [187] created engineered heart tissue construct made from heart cells, liquid collagen I, and Matrigel as well as growth

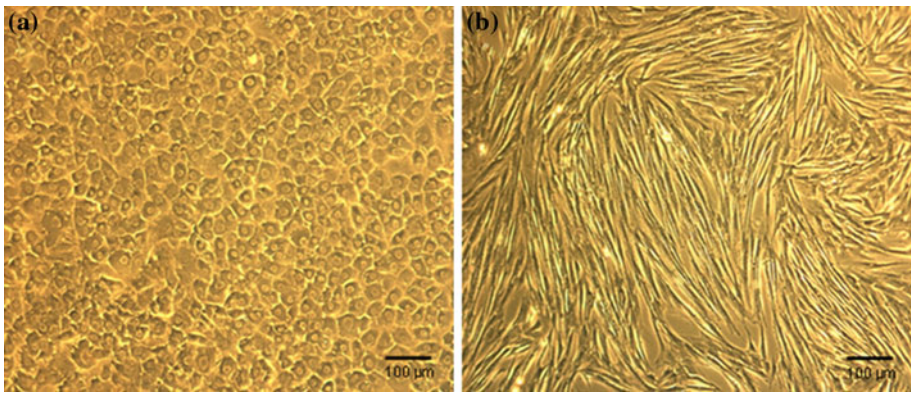

Fig. 32 Cardiomyocytes cultured in Dulbecco's Modified Eagles Medium. **a** Rat cardiomyocytes. **b** Mesenchymal stem cells

supplements, reconstituted in circular molds for the regeneration of diseased myocardium [187]. Our objective is to fabricate poly (L-lactic acid)-*co*-poly (ε-caprolactone) (70:30) and polycaprolactone/collagen (1:1) NF scaffolds (Fig. 33) modified with vascular endothelial growth factor, stromal derived factor-1, and antioxidants (ascorbic acid) for the normal functioning of left ventricular (LV) function in MI.

Injectable biomaterials for MI

The greatest advantage of injectable biomaterials is the opportunity to mix the cells and biologically active molecules prior to implantation for the regeneration of myocardial tissue. These materials which are thermally responsive biopolymer hydrogels are particularly attractive for the injection therapy following MI since it is possible to inject the necessary fluid volumes from a syringe maintained below body temperature. Upon injection of the thermoresponsive polymers, the mechanical property of the materials at the injection site is to facilitate mechanical benefit to increase the thickness of cardiac wall of the infarcted heart. Bio-absorbable thermoresponsive polymer systems have been achieved by incorporation of biodegradable segments such as hyaluronic acid, alginate, fibrin, peptides, collagen, and poly(NIPAAm-co-AAc-co-HEMAPTMC) hydrogel [175, 188]. This in situ approach utilizes an injectable biomaterial to deliver cells directly into the infarct wall to increase cell survival. An injectable treatment is more minimally invasive than implanting in vitro-engineered tissue or an epicardial patch, and is, therefore, more clinically appealing. Venugopal et al. have fabricated an injectable photopolymerized gelatin hydrogels with mesenchymal stem cells/cardiomyocytes for MI (Fig. 34). Christman et al. [189] demonstrated improved cell survival when transplanted cells are delivered in an injectable biopolymer fibrin glue to induced neovascularization within the ischemic myocardium and reduced infarct expansion [189]. Ryu et al. [190] further demonstrated the beneficial effects of an injectable fibrin glue scaffold by injecting bone marrow mononuclear cells in the matrix [190]. Kofidis et al. [191] examined an in situ approach using Matrigel® to deliver mouse embryonic stem cells [191]. An LV pouch was formed, similar to their study using an in vitro approach, and the gel was injected into the infracted area. They demonstrated improved LV function in those animals that received the Cell–Matrigel mixture compared to those that received either the biomaterial alone or cells-in-cell culture medium. Davis et al. [192] developed a novel injectable scaffold for myocardium using self-assembling peptides, which form NFs upon injection, creating a microenvironment that is suitable for

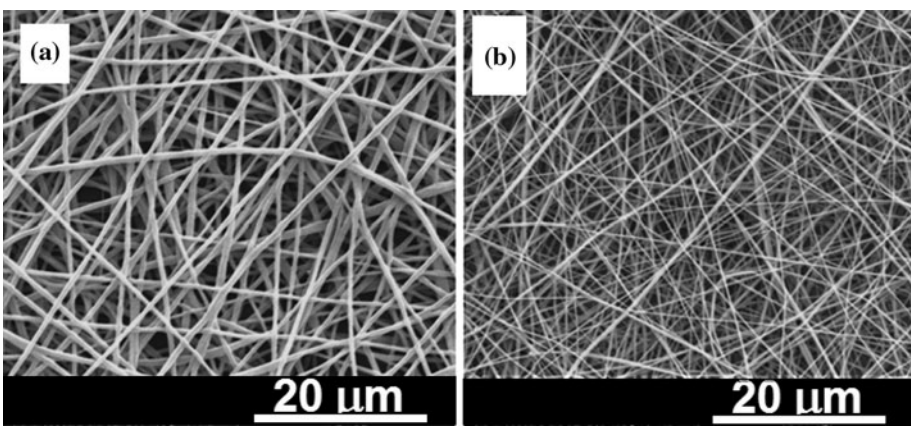

Fig. 33 Electrospun NFs. **a** Poly (l-lactic acid)-co-poly (ε-caprolactone) (10%, fiber diameter 436 ± 76 nm). **b** Polycaprolactone/collagen (10%, fiber diameter 267 ± 56 nm)

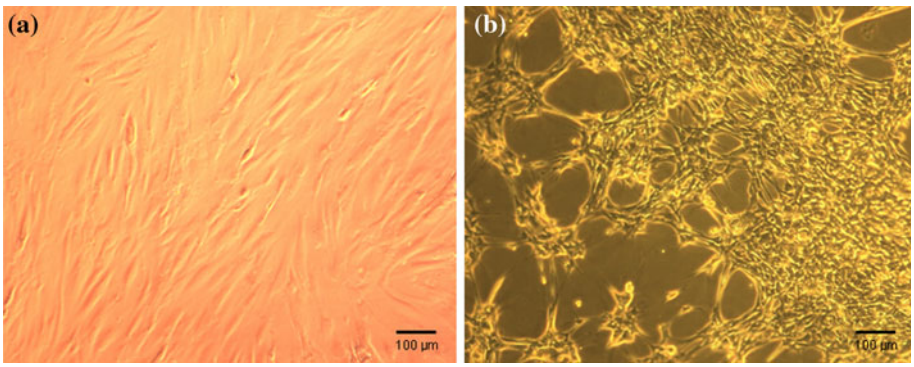

Fig. 34 Cardiomyocytes and mesenchymal stem cells cultured in gelatin hydrogel (day 5). **a** Mesenchymal stem cells, **b** Rabbit cardiomyocytes

cell and vessel ingrowth [192]. After injection of the peptides alone into infarct, progenitor cells expressing endothelial cell markers and vascular smooth-muscle cells were recruited into the NFs. Such a noninvasive scaffold may prevent heart failure by increasing the mechanical strength of the infarct, thereby preventing remodeling and deterioration of cardiac function in a similar fashion to LV restraints. Overall, design and fabrication of a noninvasive catheter-based strategy of injectable bioresorbable implant biomaterials/cells into the infarct myocardium is the feasible way to prevent mechanical complications and heart failure to save patient's life.

Summary

Before E-spinning was identified as a process for fabricating NFs, studies on nanotopographical effect on cellular response are mainly restricted to basic research with limited clinical applications. However, within the last decade, NFs have attracted attention both from researchers and clinicians due to the ease of fabrication. Today, tissue engineering and regeneration continues to dominate the use of E-spun NFs. Significant advances have been made in the construction of nerve and bone regenerative scaffold. Patterning of NF architecture by aligned, random, spiral form could fabricate biocompatible scaffolds for myocardial tissue engineering. Hybrid constructs combining biocompatible materials with stem cells as injectables are the successful noninvasive approaches for cardiac regeneration. Already, some clinical trials have been carried out to test the safety and efficacy of NFs. FDA has not given a clear definition on nanotechnology, and its long-term toxicity effects remain unknown. The unique characteristics of nanoparticles and nanomaterials are responsible for their toxicity and interaction with biological macromolecules within the human body. Nanotechnology has achieved tremendous progress in a relatively short time period in medical applications. Nanoceramics are commercially available as new bone grafts or as implant coating materials (i.e., nano-HA paste-Ostim® from Obernburg, Germany, nano-beta-tricalcium phosphate-Vitoss from Orthovita, USA). Electrospun NFs' effects are greatly reduced due to their significant length and also not being able to cross the serous membrane. Numerous in vivo studies have yet to report migration of NFs away from the immediate vicinity. In the foreseeable future, biomedical devices made of NFs or with NF components can be expected.

Drawbacks of electrospinning

Although E-spinning is established as a scalable process to fabricate random and aligned fibers of a wide range of organic and inorganic materials using multi-needle arrays and needle-less E-spinning introduced by Elmarco Inc. for a wide range of applications including the three types described here, it suffers from several limitations. Formation of nanosized fibers requires lower feed rate of the solution; which imposes severe drawbacks for their economic production at commercial scales compared to the conventional submicron fiber producing techniques such as melt blowing and island-in-the-sea processes. Although E-spinning has been scaled up at an industrial level and used commercially, notably in Donaldson high performance filters, the cost of producing them using E-spinning is still unattractive to compete with the larger diameter fibers. Other competing fiber spinning technologies such as melt blowing and island-in-the-sea process have shown to give greater yield. However, in terms of simplicity of producing long, continuous strands of relatively high quality NFs of uniform diameter, E-spinning is still the preferred technology.

Similar to many top-down techniques, E-spinning also suffers from the difficulty of achieving diameter of $\leq$10 nm. In other words, a continuous quantum wire using E-spinning has not been reported till today. The diameters of majority of E-spun polymeric fibers are still in the 100–500 nm range while inorganic NFs could be $\sim$20 nm in diameter which provide opportunities for quantum wires. While long strands of NFs can be easily fabricated using

E-spinning, 1D nanostructures with controlled aspect ratio are difficult to fabricate and often require post-spinning processes.

Although E-spun aligned NFs are consistently produced in the laboratory using simple modified setup, this has not been shown to be feasible for production at an industrial level. Extreme precise deposition of NFs for rapid prototyping to lay down structures using E-spinning has yet to be demonstrated due to the difficulty in controlling the E-spinning jet. Nevertheless, there has been steady progress in achieving precision E-spinning. Several advanced applications such as solar cells and sensors requires the 1D nanostructures to be patterned vertically on a substrate, which appears to be a major challenge for the E-spinning community. The difficulty in controlling the unsymmetrical bending required for fiber diameter reduction and removal of the momentum of the fibers upon reaching the collector substrates are issues that need to be addressed and solved.

Concluding remarks

E-spinning has been emerging as an acceptable technology for fabrication of 1D nanostructures for a number of material systems including polymers, metals, inorganic non-metals such as carbon fibers, metal oxides, carbides, and organic–inorganic composites. The E-spinning timeline since its initial discovery and potential applications of E-spun NFs are presented in this article. Conventionally, the E-spinning process is a top-down nanofabrication technique; however, the E-spun polymeric NFs act as a template for the fabrication of 1D nanostructures of inorganic materials through bottom-up principles. E-spun NFs combine a number of physical properties such as high mechanical strength, high degree of flexibility, channeled charge transport, occurrence of partially depleted space charge region, strain-induced electronic properties, large specific surface area, tailorable crystallinity, high electron and thermal diffusivity, tailorable pore-distribution, and so on. Our laboratory has been involved in fabrication of E-spun polymeric, inorganic, and polymer–nanocomposite fibers in random, aligned, cross-aligned, sheaths, tubes, yarns, core/shell, and trilayer morphologies.

Owing to the never-ending need for cleaner energy, water, and regenerative medicine, E-spun NFs are used globally to find solutions for these issues. The guided electron transport, availability of space charge-depleted space charge region, and enhanced electron diffusivity of electrons were utilized to fabricate 3D with high photoelectric conversion efficiency in limited number of fabrication steps. Similar efficiencies were achieved otherwise, e.g., using nanoparticles, involveing complex multi-step processes. Peculiar pore size distribution and tailorable crystallinity made E-spun NF-based LIBs to perform longer durations without appreciable loss of capacity.

Owing to the adjustable pore size distribution by tailoring the fiber diameter and morphology, E-spun NF membranes are used in emerging separating technology in water filtration. The pore sizes of the membranes prepared could be adjusted by altering the E-spinning conditions and through surface modification techniques like plasma-induced grafting, interfacial polymerization, and surface coating. The water flux of the grafted E-spun NF membranes has been found to be higher than that of commercial membranes. Nanofiltration membrane has been fabricated through interfacial polymerization on the surface of the E-spun NF membranes. The composite membrane was able to separate approximately 80% of divalent salts and 60% of monovalent salts.

E-spinning is a simple technology to mimic the architecture of natural extracellular matrix, and higher-order constructs for regenerating tissues such as bone and nerve have also been fabricated using E-spinning. E-spinning can also be used to integrate NFs with existing medical devices such as stent, and innovative application of E-spun NFs have been explored in cardiac tissue engineering. While bone and nerve regenerative scaffold aims to bridge a critical size defect and injury, cardiac tissue engineering aims to design and fabricate noninvasive, non-immunogenic, and biocompatible cardiac patch/injectables for the repair of myocardial infarction.

It is worth noting here that the environmental/biological hazards of nanomaterials are a major issue for their application in regenerative medicine even though nanoceramics are commercially available as new bone grafts or as implant coating materials (i.e., nano-HA paste-Ostim® from Obernburg, Germany, nano-beta-tricalcium phosphate-Vitoss from Orthovita, USA). The smaller size of some nanomaterials, such as quantum dots, can easily permeate through the serous membrane and can cause hazardous effects depending on their chemistry. Much research is currently conducted worldwide on nanotoxicology. However, continuous network of E-spun nanofibrous structure imposes serious constraints to cross the serous membrane. Nevertheless, numerous in vivo studies have yet to report migration of NFs away from the immediate vicinity.

E-spinning is a technology that world researches and innovators are now realizing and taking advantage.

Acknowledgements Authors acknowledge fellow colleagues at the Healthcare and Energy Materials Laboratory, Nanoscience and Nanotechnology Initiative, National University of Singapore. Photovoltaic and lithium ion battery researches are supported by the National Research Foundation, Singapore through the clean energy program office (NRF-CRP4-2008-03) and Competitive Research Project (NRF2007EWT-CERP01-0531). The clean water program is

supported by the Environment and Water Industry (EWI) Development Council, Government of Singapore through the funded project "*Development of low pressure, high flux UF and NF membranes based on electrospun nanofibers for water treatment* (*EDB* (*EWI*)-*0601-IRIS-062-04*)". The clean regenerative medicine program is supported by NRF—Technion project (R-398-001-063-281).

References

1. Reneker DH, Yarin AL (2008) Polymer 49:2387
2. Greiner A, Wendorff JH (2007) Angew Chem 46:5670
3. Teo WE, Ramakrishna S (2006) Nanotechnol 17:R89
4. Teo WE, Ramakrishna S (2009) Compos Sci Technol 69:1804
5. Reneker DH, Chun I (1996) Nanotechnology 7:216
6. Ramasheshan R, Sundarrajan S, Jose R, Ramakrishna S (2007) J Appl Phys 102:111101
7. Sigmund W, Yuh J, Park H, Maneeratana V, Pyrgiotakis G, Daga A, Taylor J, Nino JC (2006) J Am Ceram Soc 89:395
8. Cooley JF (1902) Apparatus for electrically dispersing fluids. US Patent Specification 692631
9. Li D, Xia YN (2004) Adv Mater 16:1151
10. Zhou ZH, Gao XS, Wang J, Fujihara K, Ramakrishna S, Natarajan V (2007) Appl Phys Lett 90:052902
11. Lee BH, Song MY, Jang S-Y, Jo SM, Kwak S-Y, Kim DK (2009) J Phys Chem C 113:21435
12. Jose R, Kumar A, Thavasi V, Fujihara K, Uchida S, Ramakrishna S (2008) Appl Phys Lett 93:023125
13. Ramakrishna S, Ng DJT (2009) Changing face of Innovation: is it Shifting to Asia. World Scientific Publishers, Singapore
14. Lewis NS, Crabtree GW, Nozik AJ et al (Eds) (2005) Basic energy sciences workshop on solar energy utilization. Office of Science, U.S. Department of Energy, Washington, DC
15. Kim MG, Cho J (2009) Adv Funct Mater 19:1
16. Simon P, Gogotsi Y (2008) Nat Mater 7:845
17. Gregg BA (2003) J Phys Chem B 107:4688
18. Grätzel M (2003) Nature 414:338
19. Yu G, Gao J, Hummelen JC, Wudl F, Heeger AJ (1995) Science 270:1789
20. Vogel R, Pohl K, Weller H (1990) Chem Phys Lett 174:241
21. Ito S, Murakami TN, Comte P, Liska P, Gratzel C, Nazeeruddin MK, Gratzel M (2008) Thin Solid Films 516:4613
22. Jose R, Thavasi V, Ramakrishna S (2009) J Am Ceram Soc 92:289
23. Thavasi V, Renugopalakrishnan V, Jose R, Ramakrishna S (2009) Mater Sci Eng R Rep 63:81
24. Green MA, Emery K, Hishikawa Y, Warta W (2009) Progr Photovolt 17:320
25. Morooka M, Noda K (2008) In: 88th spring meeting of the chemical society of Japan, Tokyo
26. Han L, Fukui A, Fuke N, Koide N, Yamanaka R (2006) In: 4th world conference on photovoltaic energy conversion (WCEP-4), Hawai
27. McConnell RD (2002) Renew Sustain Energy Rev 6:271
28. Bisquert J (2008) Phys Chem Chem Phys 10:49
29. Bisquert J (2008) Phys Chem Chem Phys 10:3175
30. Bisquert J, Fabregat-Santiago F, Mora-Sero I, Garcia-Belmonte G, Barea EM, Palomares E (2008) Inorg Chim Acta 361:684
31. Bisquert J, Garcia-Belmonte G, Bueno P, Longo E, Bulhões LOS (1998) J Electroanal Chem 452:229
32. Bisquert J, Garcia-Belmonte G, Fabregat-Santiago F, Ferriols NS, Bogdanoff P, Pereira EC (2000) J Phys Chem B 104:2287
33. Bisquert J, Gratzel M, Wang Q, Fabregat-Santiago F (2006) J Phys Chem B 110:11284
34. Bisquert J, Zaban A, Greenshtein M, Mora-Sero I (2004) J Am Chem Soc 126:13550
35. Jose R, Zhanpeisov NU, Fukumura H, Baba Y, Ishikawa M (2006) J Am Chem Soc 128:629
36. Fisher AC, Peter LM, Ponomarev EA, Walker AB, Wijayantha KGU (2000) J Phys Chem B 104:949
37. Adachi M, Jiu J, Isoda S (2007) Curr Nanosci 3:285
38. Enache-Pommer E, Boercker JE, Aydil ES (2007) Appl Phys Lett 91:3
39. Paulose M, Shankar K, Varghese OK, Mor GK, Grimes CA (2006) J Phys D Appl Phys 39:2498
40. Varghese OK, Paulose M, Grimes CA (2009) Nat Nanotechnol 4:592
41. Mukherjee K, Teng TH, Jose R, Ramakrishna S (2009) Appl Phys Lett 95:012101
42. Jennings JR, Ghicov A, Peter LM, Schmuki P, Walker AB (2008) J Am Chem Soc 130:13364
43. Li D, Xia Y (2003) Nano Lett 3:555
44. Wang C, Tong Y, Sun Z, Xin Y, Yan E, Huang Z (2007) Mater Lett 61:5125
45. Madhugiri S, Sun B, Smirniotis PG, Ferraris JP, Balkus KJ (2004) Micropor Mesopor Mater 69:77
46. Macías M, Chacko A, Ferraris JP, Balkus Jr KJ (2005) Micropor Mesopor Mater 86:1
47. Nuansing W, Ninmuang S, Jarernboon W, Maensiri S, Seraphin S (2006) Mater Sci Eng B 131:147
48. Kumar A, Jose R, Fujihara K, Wang J, Ramakrishna S (2007) Chem Mater 19:6536
49. Rinaldi M, Ruggieri F, Lozzi L, Santucci S (2009) J Vac Sci Technol B 27:1829
50. Wang Y, Jia WZ, Strout T, Schempf A, Zhang H, Li BK, Cui JH, Lei Y (2009) Electroanalysis 21:1432
51. Wang Y, Jia WZ, Strout T, Ding Y, Lei Y (2009) Sensors 9:6752
52. Wal RLV, Berger GM, Kulis MJ, Hunter GW, Xu JC, Evans L (2009) Sensors 9:7866
53. Qi Q, Feng YL, Zhang T, Zheng XJ, Lu GY (2009) Sens Actuators B Chem 139:611
54. Reddy MV, Jose R, Teng TH, Chowdari BVR, Ramakrishna S (2010) Electrochim Acta 55:3109
55. Lu HW, Zeng W, Li YS, Fu ZW (2007) J Power Sour 164:874
56. Zhang XW, Xu SY, Han GR (2009) Mater Lett 63:1761
57. Yang Y, Wang HY, Li X, Wang C (2009) Mater Lett 63:331
58. Im JS, Il Kim M, Lee YS (2008) Mater Lett 62:3652
59. Lee SH, Sigmund WM (2006) J Nanosci Nanotechnol 6:554
60. Jose R, Kumar A, Thavasi V, Ramakrishna S (2008) Nanotechnol 19:424004
61. Fujihara K, Kumar A, Jose R, Ramakrishna S, Uchida S (2007) Nanotechnol 18:365709
62. Onozuka K, Ding B, Tsuge Y, Naka T, Yamazaki M, Sugi S, Ohno S, Yoshikawa M, Shiratori S (2006) Nanotechnol 17:1026
63. Song MY, Ahn YR, Jo SM, Kim DY, Ahn JP (2005) Appl Phys Lett 87:113113
64. Song MY, Kim DK, Ihn KJ, Jo SM, Kim DY (2005) Synth Met 153:77
65. Kokubo H, Ding B, Naka T, Tsuchihira H, Shiratori S (2007) Nanotechnol 18:165604
66. Chuangchote S, Sagawa T, Yoshikawa S (2008) Appl Phys Lett 93:033310
67. Archana PS, Jose R, Vijila C, Ramakrishna S (2009) J Phys Chem C 113(52)21538–21542
68. ICDD Powder Diffraction Database. PDF#211272 (Ed) PCPDFWIN, PDF#211272
69. ICDD Powder Diffraction Database. PDF#211276 (Ed) PCPDFWIN, PDF#211276

70. Orendorz ABA, Losch J, Bai LH, Chen ZH, Le YK, Ziegler C, Gnaser H (2006) Surf Sci 600:4347
71. Banfield HZaJF (2000) J Mater Res 15:437
72. Ranade ANMR, Zhang HZ, Banfield JF, Elder SH, Zaben A, Borse PH, Kulkarni SK, Doran GS, Whitfield HJ (2001) Proc Nat Acad Sci 99(Suppl. 2):6476–6481
73. Ding XZ, Liu XH, He YZ (1996) J Mater Sci Lett 15:1789
74. Song MY, Kim DK, Ihn KJ, Jo SM, Kim DY (2004) Nanotechnol 15:1861
75. Rui Z, Jiang CY, Liu X, Liu B, Kumar A, Ramakrishna S (2008) Appl Phys Lett 93:013102
76. Shim HS, Na SI, Nam SH, Ahn HJ, Kim HJ, Kim DY, Kim WB (2008) Appl Phys Lett 92:183107
77. Wang Q, Ito S, Grätzel M, Fabregat-Santiago F, Mora-Sero I, Bisquert J, Bessho T, Imai H (2006) J Phys Chem B 110:25210
78. Zaban A, Greenshtein M, Bisquert J (2003) Chemphyschem 4:859
79. Kopidakis N, Benkstein KD, van de Lagemaat J, Frank AJ, Yuan Q, Schiff EA (2006) Phys Rev B 73:045326
80. Nair AS, Jose R, Shengyuan Y, Ramakrishna S (unpublished results)
81. Drew C, Wang XY, Senecal K, Schreuder-Gibson H, He JN, Kumar J, Samuelson LA (2002) J Macromol Sci A 39:1085
82. Senecal KJ, Ziegler DP, He JN, Mosurkal R, Schreuder-Gibson H, Samuelson LA (2001) Mater Res Soc Symp Proc 708:BB9.5.1
83. Gratzel M (2001) Nature 414:338
84. Armand M, Tarascon JM (2008) Nature 451:652
85. Tarascon JM, Armand M (2001) Nature 414:359
86. Bruce PG, Scrosati B, Tarascon JM (2008) Angewandte Chemie-Int Ed 47:2930
87. Kim JR, Choi SW, Jo SM, Lee WS, Kim BC (2004) Electrochim Acta 50:69
88. Choi SS, Lee YS, Joo CW, Lee SG, Park JK, Han KS (2004) Electrochim Acta 50:339
89. Kim JR, Choi SW, Jo SM, Lee WS, Kim BC (2005) J Electr Chem 152:A295
90. Gu YX, Chen DR, Jiao ML (2005) J Phys Chem B 109:17901
91. Shao CL, Yu N, Liu YC, Mu RX (2006) J Phys Chem Solids 67:1423
92. Zhan SH, Li Y, Yu HB (2008) J Dispers Sci Technol 29:702
93. Lu HW, Yu L, Zeng W, Li YS, Fu ZW (2008) Electrochem Solid State Lett 11:A140
94. Kim C, Yang KS, Kojima M, Yoshida K, Kim YJ, Kim YA, Endo M (2006) Adv Funct Mater 16:2393
95. Wang L, Yu Y, Chen PC, Chen CH (2008) Scripta Mater 58:405
96. Lu HW, Li D, Sun K, Li YS, Fu ZW (2009) Solid State Sci 11:982
97. Fan X, Zou L, Zheng YP, Kang FY, Shen WC (2009) Electrochem Solid State Lett 12:A199
98. Ban CM, Chernova NA, Whittingham MS (2009) Electrochem Commun 11:522
99. Fan Q, Whittingham MS (2007) Electrochem Solid State Lett 10:A48
100. Viet AL, Reddy MV, Jose R, Chowdari BVR, Ramakrishna S (2010) J Phys Chem C 114:664
101. Le Viet A, Reddy MV, Jose R, Chowdari BVR, Ramakrishna S (unpublished results)
102. Gu YX, Jian FF, Wang X (2008) Thin Solid Films 517:652
103. Ding YH, Zhang P, Long ZL, Jiang Y, Huang JN, Yan WJ, Liu G (2008) Mater Lett 62:3410
104. Brennan MB (2001) Chem Eng News 79:32
105. Baker RW, Ruthven DM (1997) Encycl Sep Technol 2:1212
106. Starthmann H, Bungay PM, Lonsdale HK, de Pinho MN (eds) (1983) Kluwer Academic Publishers, Dordrecht; Boston
107. Pinnau I, Freeman BD (eds) (2000) Formation and modification of polymeric membranes. American Chemical Society, Washington DC
108. Baker RW (2004) Membrane technology and applications, 2nd edn. John Wiley & Sons. Ltd, Chichester
109. Formhals A (1943) US Patent
110. Baumgarten PK (1971) J Colloid Interface Sci 36:71
111. Jaeger R, Schoenherr H, Vansco G (1996) J Macromol 29:7634
112. Reneker DH, Yarin AL, Fong H, Koombhongse S (2000) J Appl Phys 87:4531
113. Huang ZM, Zhang YZ, Kotaki M, Ramakrishna S (2003) Compos Sci Technol 63:2223
114. Hajra MG, Mehta K, Chase GG (2003) Sep Purif Technol 30:79
115. Gibson PW, Schreuder-Gibson HL, Rivin D (1999) Aiche J 45:190
116. Schreuder-Gibson H, Gibson P, Senecal K, Sennett M, Walker J, Yeomans W, Ziegler D, Tsai PP (2002) J Adv Mater 34:44
117. Gibson P, Schreuder-Gibson H, Rivin D (2001) Colloid Surf A-Physicochem Eng Aspect 187:469
118. Kim JS, Reneker DH (1999) Polym Eng Sci 39:849
119. Bergshoef MM, Vancso GJ (1999) Adv Mater 11:1362
120. Fong H (2004) Polymer 45:2427
121. Matthews JA, Wnek GE, Simpson DG, Bowlin GL (2002) Biomacromolecules 3:232
122. Yoshimoto H, Shin YM, Terai H, Vacanti JP (2003) Biomaterials 24:2077
123. Xu CY, Inai R, Kotaki M, Ramakrishna S (2004) Biomaterials 25:877
124. Min BM, Lee G, Kim SH, Nam YS, Lee TS, Park WH (2004) Biomaterials 25:1289
125. Shin M, Ishii O, Sueda T, Vacanti JP (2004) Biomaterials 25:3717
126. Kumar S, Dang TD, Arnold FE, Bhattacharyya AR, Min BG, Zhang XF, Vaia RA, Park C, Adams WW, Hauge RH, Smalley RE, Ramesh S, Willis PA (2002) Macromolecules 35:9039
127. Ma ZW, Kotaki M, Ramakrishna S (2005) J Membr Sci 265:115
128. Gopal R, Kaur S, Ma ZW, Chan C, Ramakrishna S, Matsuura T (2006) J Membr Sci 281:581
129. Nunes SP, Peinemann KV (2001) Membrane technology in the chemical industry. Wiley-VCH, Weinheim, Germany
130. Gopal R, Ma Z, Kaur S, Ramakrishna S, Manssori AG, George TF, Zhang G, Assoufid L (Eds) (2006) Surface modification and application of functionalized polymer nanofibers. Springer, New York
131. Chan CM, Ko TM, Hiraoka H (1996) Surf Sci Rep 24:3
132. Kaur S, Ma Z, Gopal R, Singh G, Ramakrishna S, Matsuura T (2007) Langmuir 23:13085
133. Kaur GSS, Gopal R, Barhate RS, Ng WJ, Matsuura T, Ramakrishna S, Unpublished work
134. Dong Y, Yong T, Liao S, Chan CK, Ramakrishna S (2008) J R Soc Interface/R Soc 5:1109
135. Teo WE, He W, Ramakrishna S (2006) Biotechnol J 1:918
136. He W, Yong T, Teo WE, Ma ZW, Ramakrishna S (2005) Tissue Eng 11:1574
137. Nur-E-Kamal A, Ahmed I, Kamal J, Schindler M, Meiners S (2005) Biochem Biophys Res Commun 331:428
138. Fan X, Zou R, Zhao Z, Yang P, Li Y, Song J (2009) Tissue Cell 41:266
139. Prabhakaran MP, Venugopal JR, Ramakrishna S (2009) Biomaterials 30:4996
140. Li W-J, Tuli R, Huang X, Laquerriere P, Tuan RS (2005) Biomaterials 26:5158
141. Chua K-N, Chai C, Lee P-C, Tang Y-N, Ramakrishna S, Leong KW, Mao H-Q (2006) Biomaterials 27:6043
142. Xie J, Willerth SM, Li X, Macewan MR, Rader A, Sakiyama-Elbert SE, Xia Y (2009) Biomaterials 30:354

143. Li W, Guo Y, Wang H, Shi D, Liang C, Ye Z, Qing F, Gong J (2008) J Mater Sci Mater Med 19:847
144. Corey JM, Lin DY, Mycek KB, Chen Q, Samuel S, Feldman EL, Martin DC (2007) J Biomed Mater Res A 83:636
145. Chew SY, Mi R, Hoke A, Leong KW (2008) Biomaterials 29:653
146. Zhong S, Teo WE, Zhu X, Beuerman RW, Ramakrishna S, Yung LYL (2006) J Biomed Mater Res A 79:456
147. Ma Z, He W, Yong T, Ramakrishna S (2005) Tissue Eng 11:1149
148. Wnek GE, Carr ME, Simpson DG, Bowlin GL (2003) Nano Lett 3:213
149. Fang X, Reneker DH (1997) J Macromol Sci B Phys B36:169
150. Lee SW, Belcher AM (2004) Nano Lett 4:387
151. Zhong S, Teo W, Zhu X, Beuerman R, Ramakrishna S, Yung L (2007) Mater Sci Eng C 27:262
152. He W, Ma Z, Yong T, Teo WE, Ramakrishna S (2005) Biomaterials 26:7606
153. Venugopal J, Vadgama P, Kumar TSS, Ramakrishna S (2007) Nanotechnol 18:055101
154. Chen J, Chu B, Hsiao BS (2006) J Biomed Mater Res A 79:307
155. Ngiam M, Liao S, Patil AJ, Cheng Z, Yang F, Gubler MJ, Ramakrishna S, Chan CK (2009) Tissue Eng A 15:535
156. Mendonca G, Mendonca DBS, Arago FJL, Cooper LF (2008) Biomaterials 29:3822–3835
157. Webster TJ, Ejiofor JU (2004) Biomaterials 25:4731–4739
158. Neves NM, Campos R, Pedro A, Cunha J, Macedo F, Reos RL (2007) Int J Nanomed 2:433
159. Gibson P, Schreuder-Gibson H (2004) INJ 13:34
160. Matsuda T, Ihara M, Inoguchi H, Kown IK, Takamizawa K, Kidoaki S (2005) J Biomed Mater Res 73A:125
161. Bini TB, Gao S, Tan TC, Wang S, Lim A, Lim BH, Ramakrishna S (2004) Nanotechnol 15:1459
162. Stitzel JD, Pawlowski J, Wnek GE, Simpson DG, Bowlin GL (2001) J Biomater Appl 16:22
163. Thomas V, Zhang X, Catledge SA, Vohra YK (2007) Biomed Mater 2:224
164. Teo WE, Kotaki M, Mo XM, Ramakrishna S (2005) Nanotechnol 16:918
165. Nottelet B, Pektok E, Mandracchia D, Tille JC, Walpoth B, Gurny R, Moller M (2008) J Biomed Mater Res A 89A:865
166. Panseri S, Cunha C, Lowery J, Del Carro U, Taraballi F, Amadio S, Vescovi A, Gelain F (2008) BMC Biotechnol 8:39
167. Chew SY, Mi R, Hoke A, Leong KW (2007) Adv Funct Mater 17:1288
168. Clements IP, Kim Y-t, English AW, Lu X, Chung A, Bellamkonda RV (2009) Biomaterials 30:3834
169. Teo WE, Gopal R, Ramaseshan R, Fujihara K, Ramakrishna S (2007) Polymer 48:3400
170. Smit E, Buttner U, Sanderson RD (2005) Polym Commun 46:2419
171. Teo WE, Liao S, Chan CK, Ramakrishna S (2008) Curr Nanosci 4:361
172. Kuraishi K, Iwata H, Nakano S, Kubota S, Tonami H, Toda M, Toma N, Matsushima S, Hamada K, Ogawa S, Taki W (2009) J Biomed Mater Res B Appl Biomater 88:230
173. Choi D, Hwang KC, Lee KY, Kim YH (2009) J Control Release 140:194
174. Beltrami AP, Barlucchi L, Torella D, Baker M, Limana F, Chimenti S, Kasahara H, Rota M, Musso E, Urbanek K, Leri A, Kajstura J, Nadal-Ginard B, Anversa P (2003) Cell 114:763
175. Wu J, Zeng F, Weisel DR, Li R-K (2009) Adv BioChem Engin/Biotechnol 114:107
176. Dib N, Dinsmore J, Lababidi Z, Diethrich E et al (2009) JACC Cardiovasc Interv 2:9
177. Menasche P, Hagege AA, Vilquin JT, Desnos M, Abergel E, Pouzet B, Bel A, Sarateanu S, Scorsin M, Schwartz K, Bruneval P, Benbunan M, Marolleau JP, Duboc D (2003) J Am Coll Cardiol 41:1078
178. McConnell PI, del Rio CL, Jacoby DB, Pavlicova M, Kwiatkowski P, Zawadzka A, Dinsmore JH, Astra L, Wisel S, Michler RE (2005) J Thorac Cardiovasc Surg 130:1001
179. Opie SR, Dib N (2006) Nat Clin Pract Cardiovasc Med Suppl 1:S42
180. Silva GV, Litovsky S, Assad JAR, Sousa ALS, Martin BJ, Vela D, Coulter SC, Lin J, Ober J, Vaughn WK, Branco RVC, Oliveira EM, He RM, Geng YJ, Willerson JT, Perin EC (2005) Circulation 111:150
181. Tomita S, Mickle DAG, Weisel RD, Jia ZC, Tumiati LC, Allidina Y, Liu P, Li RK (2002) J Thorac Cardiovasc Surg 123:1132
182. Park H, Radisc M, Lim JO, Chang BH, Vunjak-Novakovic G (2005) In Vitro Cell Dev Biol Animal 41:188
183. Omens JH (1998) Prog Biophys Mol Biol 69:559
184. Misra SK, Mohn D, Brunner TJ, Stark WJ, Philip SE, Roy I, Salih V, Knowles JC, Boccaccini AR (2008) Biomaterials 29:1750
185. Leor J, Tuvia S, Guetta V, Manczur F, Castel D, Willenz U, Petnehazy O, Landa N, Feinberg MS, Konen E, Goitein O, Tsur-Gang O, Shaul M, Klapper L, Cohen S (2009) J Am Coll Cardiol 54:1014
186. Jin JY, Jeong SI, Shin YM, Lim KS, Shin HS, Lee YM, Koh HC, Kim KS (2009) Eur J Heart Fail 11:147
187. Zimmermann WH, Melnychenko I, Wasmeier G, Didie M, Naito H, Nixdorff U, Hess A, Budinsky L, Brune K, Michaelis B, Dhein S, Schwoerer A, Ehmke H, Eschenhagen T (2006) Nat Med 12:452
188. Fujimoto KL, Ma ZW, Nelson DM, Hashizume R, Guan JJ, Tobita K, Wagner WR (2009) Biomaterials 30:4357
189. Christman KL, Vardanian AJ, Fang QZ, Sievers RE, Fok HH, Lee RJ (2004) J Am Coll Cardiol 44:654
190. Ryu JH, Kim IK, Cho SW, Cho MC, Hwang KK, Piao H, Piao S, Lim SH, Hong YS, Choi CY, Yoo KJ, Kim BS (2005) Biomaterials 26:319
191. Kofidis T, de Bruin JL, Hoyt G, Lebl DR, Tanaka M, Yamane T, Chang CP, Robbins RC (2004) J Thorac Cardiovasc Surg 128:571
192. Davis ME, Motion JPM, Narmoneva DA, Takahashi T, Hakuno D, Kamm RD, Zhang SG, Lee RT (2005) Circulation 111:442